Article

Cell

Multifunctional Natural Killer Cell Engagers Targeting NKp46 Trigger Protective Tumor Immunity

Graphical Abstract

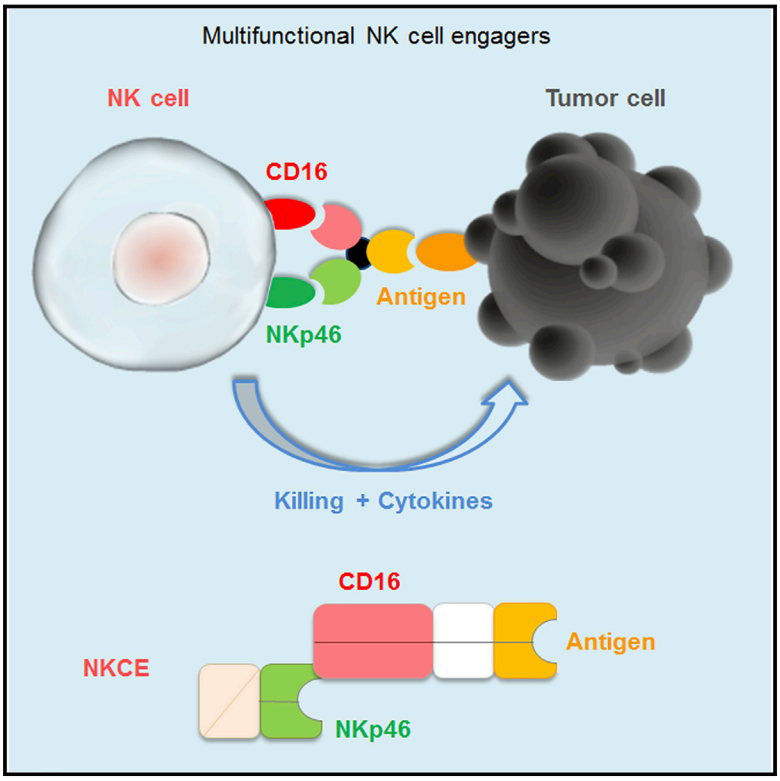

Highlights

- NK cell engagers are multifunctional Abs targeting tumor antigens, NKp46 and CD16
- NKCEs bring tumor cells and NK cells together and trigger tumor-cell destruction
- NKCEs can show killing potency superior to therapeutic Abs *in vitro* and *in vivo*
- NKCEs may improve benefit-risk profile for cancer treatment compared to BiTEs

Authors

Laurent Gauthier, Ariane Morel, Nadia Anceriz, ..., Yannis Morel, Emilie Narni-Mancinelli, Eric Vivier

Correspondence

laurent.gauthier@innate-pharma.fr (L.G.), vivier@ciml.univ-mrs.fr (E.V.)

In Brief

Trifunctional antibodies that engage natural killer cells by binding NKp46 and CD16, in addition to an antigen on cancer cells, show higher potency than current clinically available therapeutic antibodies.

Gauthier et al., 2019, Cell *177*, 1701–1713
June 13, 2019 © 2019 Elsevier Inc.
https://doi.org/10.1016/j.cell.2019.04.041

CellPress

Article

Cell

Multifunctional Natural Killer Cell Engagers Targeting NKp46 Trigger Protective Tumor Immunity

Laurent Gauthier,[1,*] Ariane Morel,[1] Nadia Anceriz,[1] Benjamin Rossi,[1] Audrey Blanchard-Alvarez,[1] Gwendoline Grondin,[1] Sylvia Trichard,[1] Cédric Cesari,[1] Melody Sapet,[1] Frédéric Bosco,[1] Hélène Rispaud-Blanc,[1] Franceline Guillot,[1] Stéphanie Cornen,[1] Alain Roussel,[2] Béatrice Amigues,[2] Guillaume Habif,[1] Flavien Caraguel,[1] Sandrine Arrufat,[1] Romain Remark,[1] François Romagné,[3] Yannis Morel,[1] Emilie Narni-Mancinelli,[4] and Eric Vivier[1,4,5,6,*]

[1]Innate Pharma, Marseille, France

[2]Aix Marseille Université, CNRS, Architecture et Fonction des Macromolécules Biologiques, Marseille, France

[3]MI-mAbs, Aix Marseille Université, Marseille, France

[4]Aix Marseille Université, INSERM, CNRS, Centre d'Immunologie de Marseille-Luminy, Marseille, France

[5]Service d'Immunologie, Marseille Immunopole, Hôpital de la Timone, Assistance Publique-Hôpitaux de Marseille, Marseille, France

[6]Lead Contact

*Correspondence: laurent.gauthier@innate-pharma.fr (L.G.), vivier@ciml.univ-mrs.fr (E.V.)

https://doi.org/10.1016/j.cell.2019.04.041

SUMMARY

Over the last decade, various new therapies have been developed to promote anti-tumor immunity. Despite interesting clinical results in hematological malignancies, the development of bispecific killer-cell-engager antibody formats directed against tumor cells and stimulating anti-tumor T cell immunity has proved challenging, mostly due to toxicity problems. We report here the generation of trifunctional natural killer (NK) cell engagers (NKCEs), targeting two activating receptors, NKp46 and CD16, on NK cells and a tumor antigen on cancer cells. Trifunctional NKCEs were more potent *in vitro* than clinical therapeutic antibodies targeting the same tumor antigen. They had similar *in vivo* pharmacokinetics to full IgG antibodies and no off-target effects and efficiently controlled tumor growth in mouse models of solid and invasive tumors. Trifunctional NKCEs thus constitute a new generation of molecules for fighting cancer.

INTRODUCTION

Immuno-oncology has emerged as a revolution in cancer treatment. In particular, immune checkpoint inhibitors (ICIs), such as therapeutic monoclonal antibodies (mAbs) directed against the PD-1 (programmed-cell death protein 1)/PD-L1 (programmed-cell death ligand 1) pathway, have been approved for use in monotherapy or combination treatments for several indications (Baumeister et al., 2016; Chen and Mellman, 2017; Okazaki et al., 2013; Okazaki and Honjo, 2007; Schumacher and Schreiber, 2015; Sharma and Allison, 2015). One of the major goals of ICI treatment is to unleash cytotoxic immune effector cells. Cytotoxicity is a key element of anti-tumor immune responses, and deficiencies of cytotoxic effector mechanisms, as in mice lacking perforin, are associated with faster-growing tumors (Smyth et al., 2000b; Street et al., 2007). Most immunomodulatory therapeutic approaches to date have focused on enhancing T cell responses, either by targeting inhibitory pathways—with ICIs, for example—or by targeting activating pathways, as with chimeric antigen receptor (CAR) T cells. CAR T cells are engineered to recognize specific tumor antigens (TAs) and have elicited unprecedented clinical responses in some hematological malignancies, such as non-Hodgkin's lymphoma, acute lymphoblastic leukemia (ALL), and chronic lymphocytic leukemia (June et al., 2018). However, CAR T cell therapy can have toxic effects, the most common being systemic cytokine response syndrome and CAR-T-cell-related encephalopathy syndrome. In parallel, bispecific T cell engagers such as BiTEs have been generated to redirect endogenous immune effector T cells to the proximity of tumors and to cluster the CD3:T cell receptor (TCR) complexes within the induced immunological synapse, triggering T cell signaling in the absence of TCR specificity (Slaney et al., 2018; Wolf et al., 2005). The success of anti-CD3 × CD19 BiTEs in B-ALL prompted the generation of many other BiTEs (Spiess et al., 2015). Like CAR T cell therapy, BiTE treatments are limited by toxicity. Furthermore, the control of solid tumors by BiTE and CAR T cell therapies remains a challenge.

Interest has recently focused on the use of natural killer (NK) cells for therapeutic interventions, as these cells have anti-tumor properties (Cerwenka and Lanier, 2018; Chiossone et al., 2018; Mittal et al., 2018). NK cells express several activating receptors that can be targeted to induce NK-cell-mediated anti-tumor immunity, such as cluster of differentiation 16 (CD16, also known as FcγRIIIA), natural killer group 2D (NKG2D), signaling lymphocyte activation molecule (SLAM)-family members, and the natural cytotoxicity receptors (NCRs) NKp30, NKp44, and NKp46 (Moretta et al., 1996, 2006; Wu and Veillette, 2016). The full activation of NK cells has been shown to require the co-engagement of different cell-surface receptors (Bryceson et al., 2009; Bryceson et al., 2006).

NKp46 (NCR1, CD335) is a 46-kDa glycoprotein belonging to the immunoglobulin (Ig) superfamily (Moretta et al., 2006). NKp46 consists of two extracellular Ig-like domains of the C2

type (Pessino et al., 1998). It is expressed by resting and activated NK cells (Sivori et al., 1997), innate lymphoid cell (ILC) 1, a small population of T lymphocytes, and a subset of ILC3 (NCR^+ ILC3) in mucosa (Vivier et al., 2018). NKp46 is highly conserved in mammals (Moretta et al., 2006) and plays a role in the NK-cell lysis of autologous, allogeneic, or xenogeneic cells (Sivori et al., 1999). NKp46 triggering mediates signaling via its association with the immunoreceptor tyrosine-based activation motif (ITAM)-bearing molecules CD3ζ and FcRγ that, upon receptor-engagement, become tyrosine phosphorylated. NKp46 mAb-mediated cross-linking triggers not only NK-cell cytotoxic activity but also cytokine release (Sivori et al., 1999). The NKp46 cellular ligands expressed on normal or tumor cells have yet to be identified, but soluble ligands and ligands of microbial origin potentially involved in the NKp46-mediated recognition of microbial infected cells have recently been described (Guia et al., 2018; Narni-Mancinelli et al., 2017). In particular, NKp46 recognizes influenza virus hemagglutinin and the parainfluenza virus hemagglutinin neuraminidase in a sialic-acid-dependent manner (Mandelboim et al., 2001).

We report here the design, production, and characterization of a new generation of trifunctional NK-cell engagers (NKCEs) consisting of mAb fragments targeting the activating NK-cell receptor NKp46, together with a TA and an Fc fragment, to promote antibody-dependent cell-mediated cytotoxicity (ADCC) via the activating receptor CD16 expressed on NK cells. NKCEs were effective against several tumor types *in vitro*, with no off-target cytotoxicity. *In vivo*, NKCEs were more potent than intact anti-TA mAbs, such as the anti-CD20 mAb rituximab and the Fc-engineered anti-CD20 mAb obinutuzumab, in mouse models of both invasive and solid tumors. These results support the clinical development of NKCEs for next-generation cancer immunotherapy.

RESULTS

NKp46 Is Expressed on NK Cells in the Tumor Bed

We investigated the expression of activating receptors on NK cells in tumor conditions, with a view to designing novel therapeutic molecules capable of triggering NK-cell effector functions. $NKp46^+$ cells were less abundant than $CD8^+$ cells in tumors, but we nevertheless identified NKp46 as frequently expressed on the lymphocytes infiltrating diverse types of human solid cancers (Figures 1A–1C). For instance, in squamous cell carcinoma of the head and neck (SCCHN), 14-color flow cytometry coupled with t-distributed stochastic neighbor-embedding (t-SNE) analysis showed that NK cells could be classified into main two subsets, referred to hereafter as clusters 1 and 2. Cluster 1 was overrepresented in tumors relative to peripheral blood (Figure S1A) and consisted of a high frequency of $NKp46^+$ cells with low levels of expression of both NKp44 and CD16 (Figure S1A). The enrichment in $CD16^{low}$ $NKp46^+$ tumor-infiltrating NK cells appeared heterogeneous, differing between patients (data not shown). Sustained NKp46 expression, associated with the downregulation of other activating receptors, such as NKG2D, NKp30, and NKp44, has been reported for other cancers, such as acute myeloid leukemia, breast cancer, and lung carcinoma (Fauriat et al., 2007; Mamessier et al., 2011; Platonova et al., 2011). The downregulation of NKG2D on both NK and T cells has been observed in many cancers (Clayton et al., 2008; Crane et al., 2010; Saito et al., 2012; Wang et al., 2008; Wu et al., 2004), including lung cancer (Figure S1B). By contrast, we observed no statistically significant downregulation of NKp46 in the periphery in SCCHN, breast, liver, lung, kidney, and metastatic melanoma cancer patients (Figures 1D and S1C; data not shown). These results thus identified NKp46 as a good candidate for the targeting of an activating receptor on NK cells in cancer.

Generation and Characterization of Anti-NKp46 mAbs

For the targeting of NKp46 in patients, we generated anti-NKp46 antibodies by immunizing mice with a recombinant soluble human NKp46-Fc molecule (Narni-Mancinelli et al., 2017). More than 200 positive hybridoma preclones were identified, and 109 of these were cloned as human IgG1 chimeric mAbs for in-depth characterization. These anti-NKp46 mAbs were then titrated on a human cell line engineered to express NKp46, selected for cross-reactivity with NKp46 from cynomolgus monkeys (*Macaca fascicularis*) for further preclinical development and then ranked on the basis of affinity. Seventeen representative mAbs were humanized by complementarity-determining region (CDR) grafting and retained for further physicochemical characterization (Figure S2; Table S1; data not shown).

These 17 anti-NKp46 mAbs (NKp46-1 to NKp46-17) were also characterized in competition studies (Figure S2). In total, we analyzed 289 (17×17) antibody combinations by surface plasmon resonance (SPR), and all but one of the pairs of mAbs displayed symmetric behavior (Figures S2A and S2B). For the mapping of their epitopes on the surface of NKp46, we used structural data for human NKp46 to generate several mutant NKp46 proteins (Foster et al., 2003; Ponassi et al., 2003) (Figure S2C; Table S1). A library of 36 mutants was generated by mutating patches of surface residues from the extracellular domain (ECD) conserved between cynomolgus monkeys and humans but not present in the mouse NKp46 molecule (mutants 1–23) and by mutating the residues conserved between all these species (mutants S1–S13). For instance, the binding of the NKp46-1 mAb was affected in mutants 2 and S7, and that of the NKp46-3 mAb was affected in mutants 19 and S8, indicating a probable role of the mutated residues in the epitopes targeted by these mAbs (Figure S2C). Epitope mapping experiments identified only eight binding sites in the 17 mAbs studied (Table S1), despite consideration of the entire surface of NKp46 (Figure S2C). The mutation of larger areas significantly impaired NKp46 folding, preventing further analysis (data not shown). Based on these results, we were able to establish a coherent epitope diagram (Figure S2D). Anti-NKp46 mAbs were clustered into two main competitive groups on the basis of binding to NKp46-ECD domain 1 or to the C-terminal part of domain 2. The NKp46-1 mAb epitope (Figures S2C and S2D, red) was located at the transition between domains 1 and 2, at the supposed top of the molecule. The NKp46-4 mAb epitope was located in the N-terminal part of domain 1 (Figure S2D, green), whereas the epitope of the NKp46-17 mAb, which competed with all mAbs targeting domain 2, was located in the C-terminal part of domain 2 (Figure S2D, black). Fourteen of these mAbs also cross-reacted with freshly prepared cynomolgus monkey

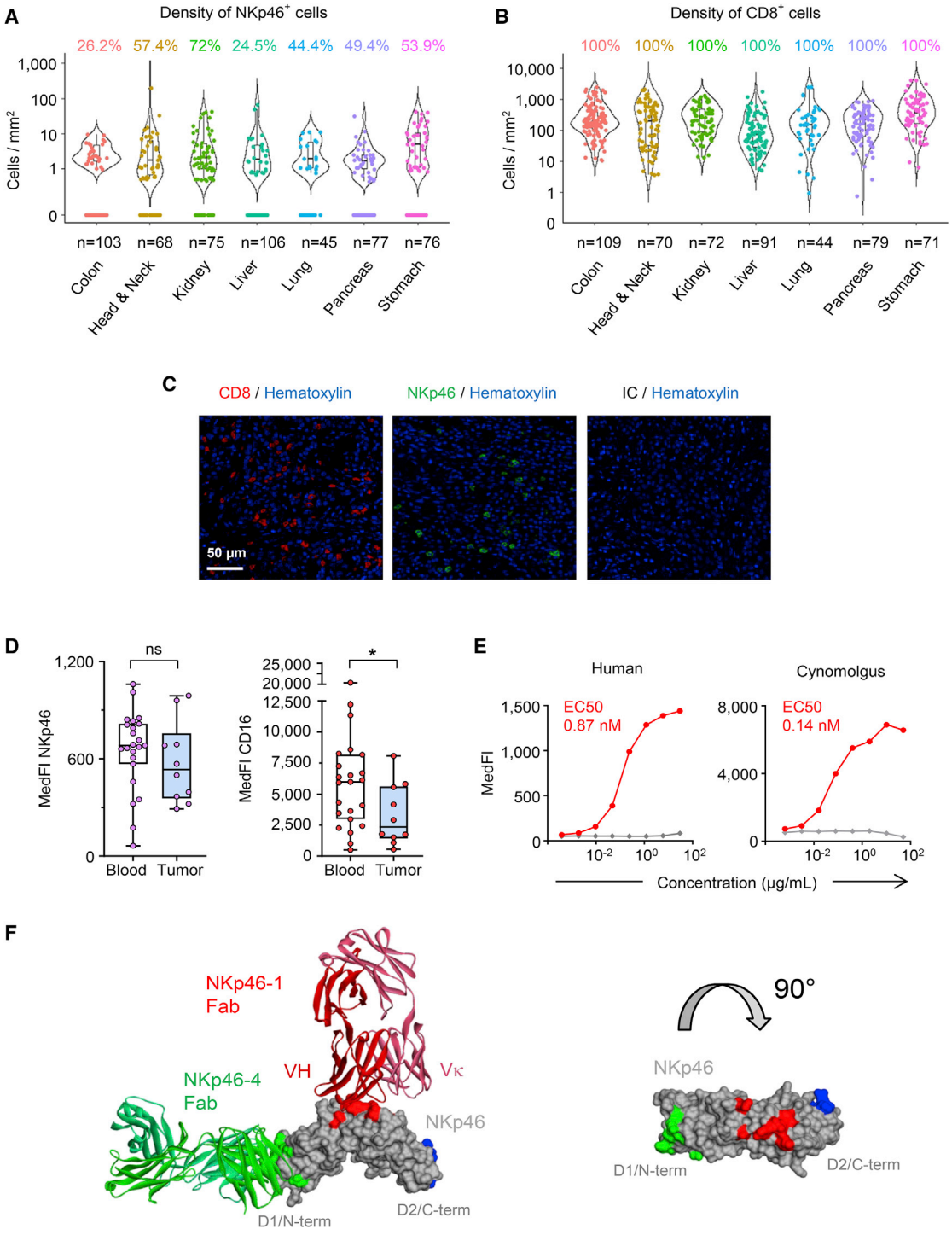

Figure 1. NKp46 Is Expressed in the Tumor Bed

(A) NKp46$^+$ cell densities in various human solid tumors. The number of tumors analyzed and the percentage of tumors positive for NKp46 are indicated.
(B) CD8$^+$ cell densities in various human solid tumors. The number of tumors analyzed is indicated. All tumors were infiltrated.
(C) Representative images of CD8 (red) and NKp46 (green) immunostaining for head and neck tumor tissues. The white scale bar corresponds to 50 µm.
(D) Median fluorescence intensity of NKp46 and CD16 staining for NK cells from peripheral blood (n = 24) and tumor tissues (n = 10) from head and neck cancer patients. Statistical test: two-way repeated measures ANOVA and Sidak's post hoc test. n events per sample > 100 (n.s., not significant. $p > 0.05$; *$p < 0.05$).
(E) Representative titration of anti-NKp46-1 mAb on NK cells purified from the PBMCs of human healthy volunteers and cynomolgus monkeys. The titration data shown are median fluorescence intensity over a range of antibody concentrations. EC_{50} values are indicated.

(legend continued on next page)

peripheral blood mononuclear cells (PBMCs) (Figure 1E; data not shown). Mouse IgG1 versions of anti-NKp46 antibodies were generated and were found to bind to human NK cells, the lowest half-maximal effective concentration (EC_{50}) being obtained with NKp46-1 (Figure 1E; data not shown). The structure of the NKp46-1 antibody Fab was solved by X-ray crystallography at a resolution of 1.7 Å and co-crystallization of the NKp46-1 and NKp46-4 mAbs with NKp46 validated both the competition and epitope mapping experiments (Figures 1F and S2D). A large library, consisting of 14 anti-NKp46 mAbs binding to different parts of the NKp46-ECD with different affinities, was thus available, making it possible to assess the various options for optimal NK-cell activation.

Generation and *In Vitro* Function of Bispecific NKCEs

We initially generated bispecific NKCE mAbs by associating anti-NKp46 Fabs with a single-chain variable fragment (scFv) directed against a TA via a monomeric Fc moiety preventing binding to CD16 (F2 format) (Ying et al., 2012) (Figure 2A). We refer to these mAbs hereafter as NKp46/(Fc)/TA-F2. Prototypic bispecific NKp46/(Fc)/CD19-F2 NKCEs binding to three different discrete NKp46 epitopes located at the N terminus (NKp46-4), C terminus (NKp46-3), and the transition between domains 1 and 2 (NKp46-1) (Figure 1F) were evaluated for their ability to promote the lysis of $CD19^+$ human Daudi B cell lymphoma cells by NK cells (Figures 2B and 2C). The various bispecific NKCEs were similarly effective at inducing NK-cell-mediated tumor lysis. In addition, all these bispecific NKCEs were more effective than the anti-CD19 IgG1 mAb used as a positive control of ADCC in this experimental setting. Even though circulating NK cells express higher levels of CD16 than of NKp46 (Figure 2B), these results suggest that engaging NKp46 could be a more efficient approach than inducing ADCC. This observation was also confirmed for tumor antigen targets other than CD19 (data not shown). The capacity of bispecific F2 NKCEs to activate NK cells was also demonstrated by the induction of the degranulation marker CD107 and the activation marker CD69 on the NK-cell surface (Figure 2D). We chose to focus on the anti-NKp46-1 mAb for the further development and characterization of NKCEs, as NKp46-1 was the best mAb for inducing NK-cell activation (Figures 2C and 2D), and its chemistry manufacturing and control (CMC) data were favorable for industrial development (data not shown).

Development of Multifunctional NKCEs

We engineered NKCEs with several different formats to adjust the pharmacologic properties of the molecule and to facilitate production and purification. All NKCE formats contained Fc or Fc-derived fragments to increase productivity and facilitate purification (Figure 3A). The NKCE library included multiple molecules displaying monovalent or bivalent binding to one or two TAs and monovalent binding to NKp46. We first focused on seven bispecific NKCEs with a silent Fc fragment, due to a monomeric Fc (Ying et al., 2012), tandem CH3, or N297S mutation (Dennler et al., 2014) (Figure 3B). In addition to F2, single-chain polypeptides (F1, F4) or multi-chain polypeptides (NKCE-1, F9, F10, F11) with different possible sites of TA binding to scFv, Fab, and Fab-like were designed. A novel affinity-driven pairing technology was used to ensure correct Fc assembly and to drive appropriate pairing of the different chains (Gauthier and Rossi, 2016). All of these formats were generated and purified, and their affinity for conventional Fcγ receptors was checked by SPR with the representative NKCE-1 format (Figures S3 and S4; data not shown).

The potential of the various formats of silent-Fc bispecific antibodies to promote NK-cell-derived tumor lysis was investigated. All the silent-Fc NKCEs were functional for NK-cell activation and displayed strong anti-tumor activity *in vitro* (Figure 3C). Among these NKCEs, the bispecific NKCE with an NKCE-1 format, with its simple molecular organization, had a high level of anti-tumor efficacy and production. NKCEs with the NKCE-1 format had IgG1-like pharmacokinetic properties *in vivo,* normal levels of binding to FcRn, and a terminal half-life of 11 days, whereas NKCEs with the F2, F4, F9, F10, and F11 formats bound to FcRn with low affinities and were cleared within hours *in vivo* (Figure 3D; data not shown). We therefore pursued our investigations with NKCEs of the bispecific anti-NKp46-NKCE-1 format, which had Fab-based antigen-binding sites and displayed CMC properties compatible with clinical development.

As cell-surface molecules other than NKp46—such as NKG2D—might also serve as potent inducers of NK-cell activation, we compared, side-by-side, the efficacy with which bispecific NKCEs targeting NKp46 and NKG2D promoted NK-cell cytolytic activity in two different *in vitro* models. In the NKCE-1 format, NKCEs targeting NKp46 promoted tumor target cell lysis by resting NK cells more efficiently than those targeting NKG2D, consistent with the level of NCR expression at the cell surface (Figure S5). Similar efficiencies of NKp46 and NKG2D NKCEs were recorded with human KHYG-1 NK cell line, although NKp46 was less strongly expressed on these cells than NKG2D. These results and the relative expression of these activating receptors in cancer patients (Figures 1 and S1) led us to focus on targeting NKp46 rather than NKG2D for the induction of NK-cell activation.

Bispecific NKCEs Promote Tumor Control *In Vivo*

We evaluated the *in vivo* efficacy of bispecific NKCEs against tumors by generating NKCE-1 bispecific NKCEs targeting the 29A1.4 epitope of mouse NKp46 (Walzer et al., 2007) and the human CD20 as a TA for targeting human Raji lymphoma B cells in a transplantable xenogeneic solid tumor model. Anti-mouse NKp46 29A1.4 mAb was a good surrogate for anti-human NKp46-1 mAb, as these two mAbs bound their cognate NKp46 antigens with similar affinities (data not shown). $CD20^+$ Raji

(F) 3D structures of NKp46-1-Fab (red/pink), NKp46-4-Fab (green), and NKp46-ECD (gray) complexes (PDB: 6IAP and 6IAS). Two antibody Fabs co-crystallized with NKp46-ECD are shown (left). NKp46-1/NKp46-ECD interface showing the position of the NKp46-1 epitope (red surface), NKp46-4 epitope (green surface), and mutants 19 and S8 (blue surface). Red, NKp46-1 VH-CH1; pink, NKp46-1 Vκ-Cκ; dark green, NKp46-4 VH-CH1; green, NKp46-4 Vκ-Cκ; gray, NKp46-ECD.

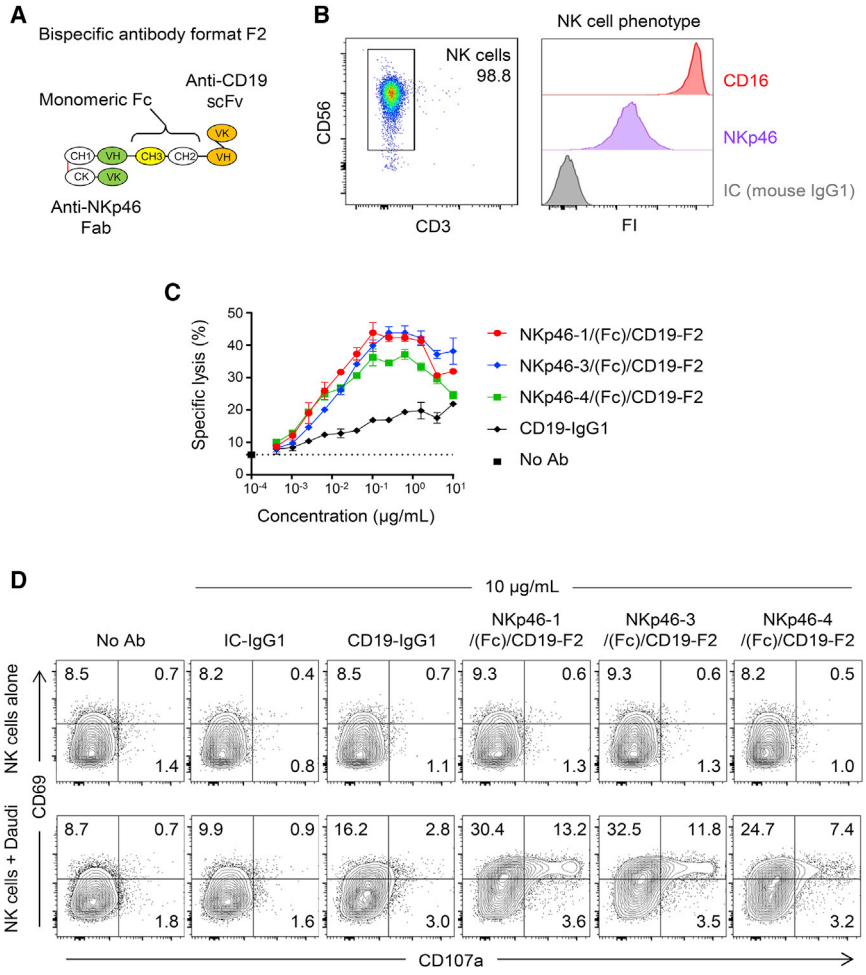

Figure 2. *In Vitro* Activity of Anti-NKp46 Antibodies Targeting Different Epitopes on NKp46

(A) Molecular design of the F2 bispecific format.

(B) Phenotype of the purified resting NK cells used in (C) and (D).

(C) Comparison of the cytotoxicities of the different NKCEs with F2 format harboring diverse epitopes differing in specificity for NKp46 and the CD19 TA. Daudi cells were used as the target and purified resting NK cells as effectors. The data shown are representative of 3 independent experiments.

(D) Experiment similar to that in (C) but with the measurement of CD69 and CD107 expression on NK cells by flow cytometry at one dose of 10 μg/mL antibody or NKCE. The percentages of CD69- and CD107-expressing NK cells are indicated. NK cells alone (upper panels) are compared with NK cells cocultured with Daudi cells (lower panels).

tumors grew progressively in 90% of engrafted CB17-severe-combined-immunodeficient (SCID) mice treated with control mAb (Figure 4A). By contrast, the tumors were controlled in around half the mice treated with NKp46/(Fc)/CD20-NKCE-1 bispecific NKCEs at doses of 0.25 and 6.25 mg/kg.

Mechanistically, we could show that NK cells were required to control tumor growth, because the administration of an anti-asialo-GM1-depleting mAb to NKCE-treated tumor-bearing mice abolished the control of Raji tumor growth (Figures 4A and S6). Thus, NKp46 activation by bispecific NKCEs led to NK-cell-dependent tumor control *in vivo*. We further dissected the mechanisms underlying the efficacy of bispecific NKCEs by monitoring the presence of tumor-infiltrating NKp46^{+} cells at various times after treatment to determine whether NKCEs could mobilize NK cells in the tumor bed. We developed an RNAscope-based assay for measuring levels of the *Ncr1* mRNA encoding mouse NKp46 without interfering with the binding of NKCEs to the NKp46 receptor. Using this protocol, we observed that NK-cell counts were about 80% higher in NKCE-treated mice than in control animals, indicating that, in addition to promoting tumor clearance, bispecific NKCE treatment promoted NK-cell infiltration and/or proliferation within tumors (Figures 4B and 4C).

Generation and *In Vitro* Characterization of Trifunctional NKCEs

We then developed other mAb formats co-engaging NKp46 with the ADCC effector pathway to improve the anti-tumor efficacy of NKCEs. We generated two trifunctional antibodies capable of co-engaging CD16 on NK cells (Figures S3 and S4). One is referred to hereafter as NKp46/Fc/TA-NKCE-2 and harbored a wild-type Fc portion. The other trifunctional NKCE (NKCE-3 format) displayed the S239D and I332E mutations, which optimized CD16 Fc receptor binding (Shields et al., 2011). We confirmed by SPR that NKp46/(Fc)/TA-NKCE-1 and NKp46/Fc/TA-NKCE-2 bound NKp46 with similar affinities (Figure S7A). We also observed that the sequential binding of Fc-competent trifunctional NKCEs to NKp46 did not interfere with subsequent binding to CD16, demonstrating that NKCEs could co-engage CD16 and NKp46 simultaneously, without steric hindrance (Figures S7B and S7C).

We assessed the anti-tumor efficacy of NKCE treatment *in vitro* by comparing NKCEs with no binding to CD16 (NKp46/(Fc)/TA-NKCE-1), wild-type binding to CD16 (NKp46/Fc/TA-NKCE-2), and enhanced binding to CD16 (NKp46/Fc*/TA-NKCE-3) (Figure 5). All these NKCE formats were developed against three different TAs: CD19 and CD20 to target Daudi human B cell lymphoma cells and EGFR to target A549 human lung carcinoma cells. Trifunctional Fc-competent NKp46/Fc/TA-NKCE-2 molecules promoted tumor-cell lysis by NK cells more effectively than Fc-silent NKp46/(Fc)/TA-NKCE-1 molecules (Figures 5A and 6A). The co-engagement of NKp46 and CD16 increased both the potency of tumor-cell lysis and NK-cell activation relative to a bispecific NKp46/(Fc)/TA-NKCE-1, regardless of the TA (Figures 5A and 6B).

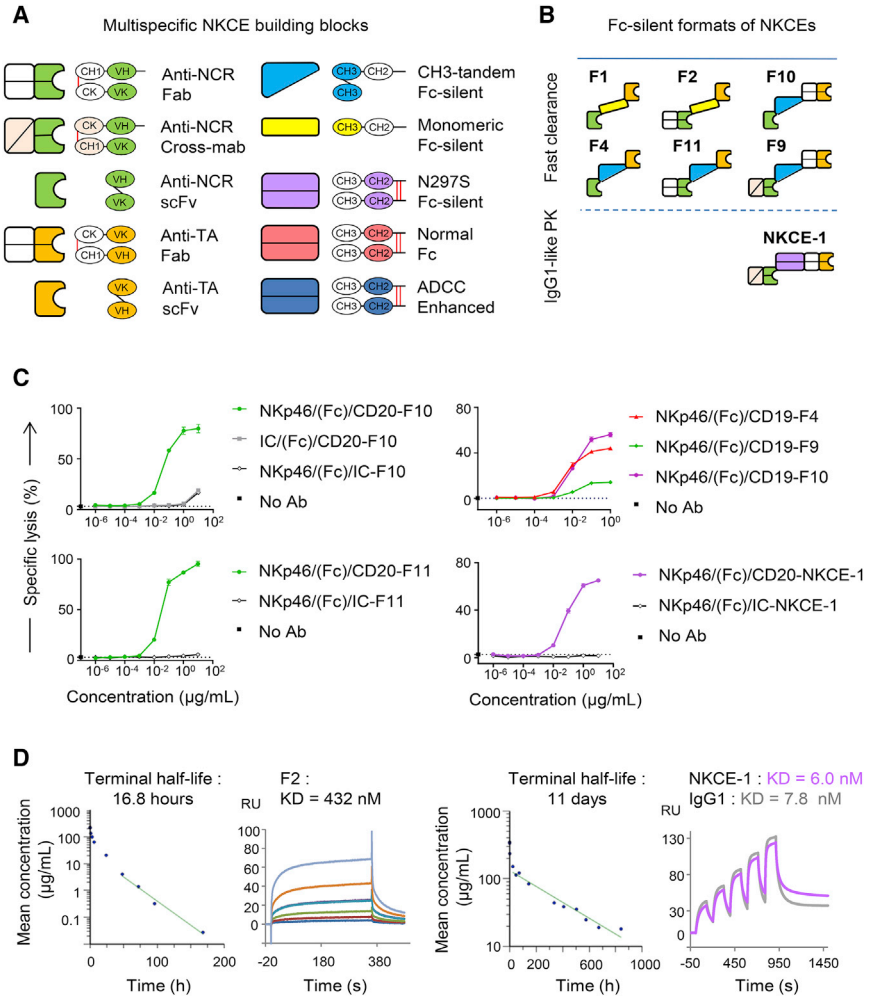

Figure 3. Development and Comparison of Silent-Fc NKCE mAb Formats *In Vitro*

(A) Design of NKCE formats.

(B) Schematic representation of Fc-silent NKCEs.

(C) Comparison of the cytotoxicities of the different NKCEs with NKp46-Fc silent formats harboring NKp46-1 epitope specificity and binding to the CD19 and CD20 TAs. Daudi cells were used as the target and purified resting NK cells as effectors. Data are representative of more than 10 independent experiments.

(D) Pharmacokinetic and FcRn binding studies of F2 (left panels) and NKCE-1 (right panels) Fc-silent NKCEs. Pharmacokinetic studies in nude mice showing mean serum concentrations of NKCEs over time (blue dots). Predicted concentrations are shown (green line). The determined terminal half-life is indicated. Data are representative of one to two experiments. SPR studies of FcRn binding: superimposed sensorgrams showing the binding of recombinant human FcRn proteins to NKp46-1/(Fc)/CD19-F2 (left) and NKp46-1/(Fc)/CD19-NKCE-1 (right) immobilized on a CM5 chip. Sensorgrams obtained after the injection of various concentrations of F2-NKCEs, from 9.4 to 300 nM, were aligned such that the start of the injection was at zero on the x and y axes. Sensorgram obtained by single-cycle kinetic analysis after the injection of various concentrations of NKCEs with a NKCE-1 format, from 17 to 272 nM, superimposed on that obtained with regular human IgG1 and aligned such that the start of the injection was at zero on the x and y axes. We fitted a 1:1 binding model to the data.

NKp46/Fc*/TA-NKCE-3, optimized for binding to CD16, further increased tumor-cell killing frequency and NK-cell activation (Figure 6). Remarkably, in all conditions tested, the optimized-Fc trifunctional NKCEs were more efficient than the intact anti-CD20 rituximab, the ADCC-enhancing anti-CD20 obinutuzumab, and the anti-EGFR cetuximab antibodies widely used in clinical practice (Figure 5A).

We also showed that the co-engagement of NKp46 and CD16 with trifunctional NKCEs potentiated NK-cell activation, as trifunctional molecules were more potent than a mixture of the bispecific reagents activating NKp46 and CD16 separately (Figure 5B). We also investigated the potential off-target activation of NK cells through the cross-linking of CD16 and NKp46 with Fc-competent trifunctional NKCEs by studying the killing of TA-negative target cells *in vitro* (Figure 5C). In this assay, we used HUT78 human cutaneous T cell lymphoma cells, which express killer cell immunoglobulin-like receptor 3DL2 (KIR3DL2) as a tumor antigen but are negative for CD19, contrasting with Daudi human B cell lymphoma cells, which are KIR3DL2^{-}CD19^{+}. We observed no killing of cells that did not express the TA targeted by the NKCEs. We also assessed *in vitro* whether the cross-linking of CD16 and NKp46 with Fc-competent trifunctional NKCEs induced NK-versus-NK toxicity (Figure 5D). We assessed the killing of Daudi cells and of NK cells in the same assay. Strong Daudi-cell killing was induced by Fc-competent trifunctional NKCEs, but we observed no NK-cell mortality, indicating that Fc-competent trifunctional NKCEs do not mediate fratricidal NK-cell killing. Taken together, these results indicate that trifunctional NKCEs can efficiently promote NK-cell-mediated tumor-cell lysis without inducing potentially toxic off-target effects or the fratricidal killing of NK cells.

Anti-tumor Function of Trifunctional NKCEs

We then assessed the *in vivo* efficacy of NKCEs. In a first series of experiments, we used a solid tumor model based on the subcutaneous (s.c.) injection of Raji B lymphoma cells. Tumor-bearing mice treated with bispecific NKCEs or trifunctional NKCEs displayed significantly greater decreases in tumor size than the control mAb-treated group, and trifunctional NKCEs were significantly more potent than obinutuzumab (Figure 7A). We complemented these results by assessing the efficacy of NKCEs in another tumor model of invasive B cell lymphoma resulting from the i.v. injection of the Raji tumor cells. Trifunctional NKCEs were more effective than

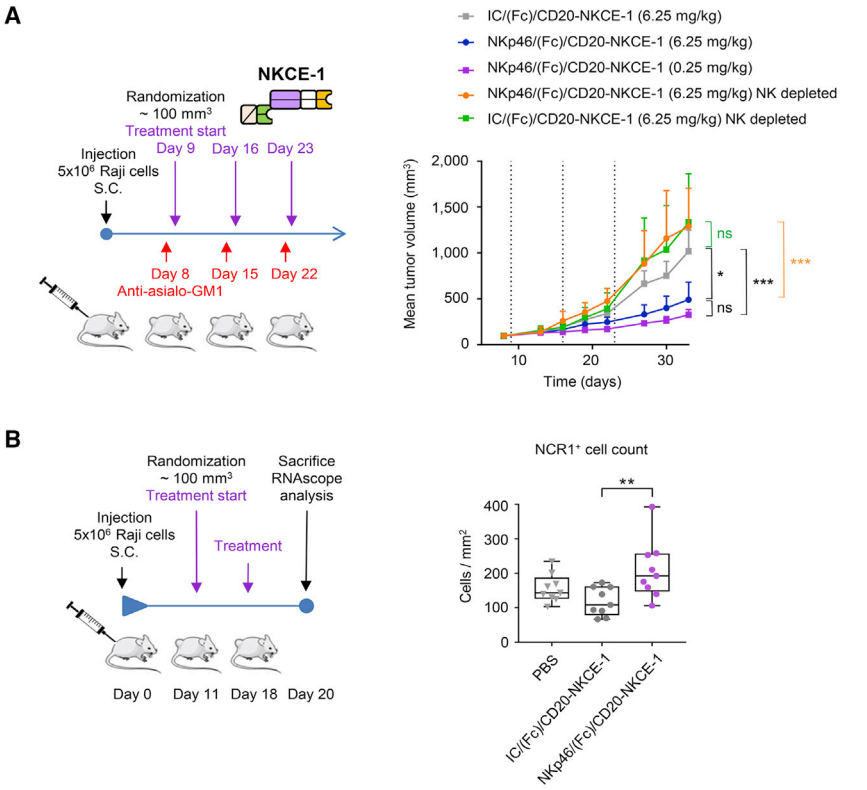

Figure 4. Bispecific NKCEs Promote Tumor Growth Control *In Vivo*

(A) Left panel: schematic diagram of the experimental setting. Raji cells were subcutaneously (s.c.) injected into mice on day 0. Tumor-bearing mice were randomized on day 8 and depleted of NK cells by anti-Asialo-GM1 conditioning once weekly for three weeks (red arrows), beginning on day 8, or were treated with control serum. Mice were also treated once weekly for three weeks with NKCEs IC/(Fc)/CD20-NKCE-1 (control group; gray; 6.25 mg/kg body weight) or NKp46/(Fc)/CD20-NKCE-1 (NKCE-treated group; blue 6.25 and purple 0.25 mg/kg body weight), beginning on day 9 (purple arrows). Right panel: mean tumor volumes ± SEM are shown. p values were calculated based on the t distribution using degrees of freedom based on Kenward-Roger method. These calculations were done with the R package lmerTest *$p < 0.05$; **$p < 0.01$; ***$p < 0.001$. ns: non-significant.

(B) Accumulation of NCR1-positive cells in the tumors of NKCE-treated animals. Mice bearing solid Raji tumors were randomized to three groups (n = 20/group) and treated twice with vehicle (PBS 1X) or with 1.25 mg/kg body weight of either IC/(Fc)/CD20-NKCE-1 or NKp46/(Fc)/CD20-NKCE-1 NKCEs. IHC/RNAscope analysis was performed to determine the numbers of NCR1-positive cells per unit of tumor section area. Kruskal-Wallis test. **$p \leq 0.01$.

(C) Representative NCR1-RNAscope staining of mice treated with IC/(Fc)/CD20-NKCE-1 (left panel) or NKp46/(Fc)/CD20-NKCE-1 (right panel). The black scale bar corresponds to 100 μm.

obinutuzumab over a range of doses, with all mice rescued from death at a dose of 50 μg of antibody per kilogram body weight versus 60% of mice rescued in the obinutuzumab-treated group (Figure 7B). These results thus constitute proof of principle for the efficacy of trifunctional NKCEs for promoting the control of tumors *in vivo*, providing support for their clinical development.

Increases in the potency of cytotoxicity could potentially be associated with higher toxicity in patients. We therefore measured the cytokine release from human PBMCs induced by CD20-NKCEs *in vitro* and compared it with that induced by ADCC-enhanced antibodies targeting CD20. PBMCs were cultured for 24 h in the presence of NKp46/Fc/IC-NKCE-2, NKp46/Fc/CD20-NKCE-2, NKp46/Fc*/IC-NKCE-3, or NKp46/Fc*/CD20-NKCE-3 NKCEs or obinutuzumab and interleukin (IL)-1β, IL-2, IL-6, IL-8, MIP-1α, MCP-1, TNF-α, and INF-γ were quantified in the supernatant. CD20-NKCEs induced barely detectable cytokine release and harbored the same cytokine profile as ADCC-enhanced anti-CD20 antibody obinutuzumab, indicating the absence of toxicity alert for NKCEs (data not shown).

DISCUSSION

Most attempts at anti-tumor therapy to date have focused on manipulating effector T cells (Chen and Mellman, 2017; Okazaki et al., 2013; Okazaki and Honjo, 2007; Schumacher and Schreiber, 2015; Sharma and Allison, 2015). We decided to manipulate NK cells in cancer immunotherapy because of their anti-tumor effector potential (Cerwenka and Lanier, 2018; Chiossone et al., 2018; Guillerey and Smyth, 2016; Rautela et al., 2018; Vivier et al., 2012). NK cells were originally defined on the basis of their ability to kill tumor cells *in vitro* (Trinchieri, 1989). This observation was confirmed in several tumor models in mice (Glasner et al., 2012; Glasner et al., 2018; Halfteck et al., 2009; Smyth et al., 2001; Smyth et al., 2000a). In humans, various studies have shown peripheral blood natural cytotoxicity to be lower in patients with various types of solid tumors than in healthy individuals (Brittenden et al., 1996). A correlation between poor NK-cell function and the development of metastases has been established in pharyngeal (Schantz et al., 1989), head and neck (Schantz et al., 1986; Schantz and Ordonez, 1991), and other solid tumors (Imai et al., 2000; Pross and Lotzová, 1993). NK-cell infiltration in

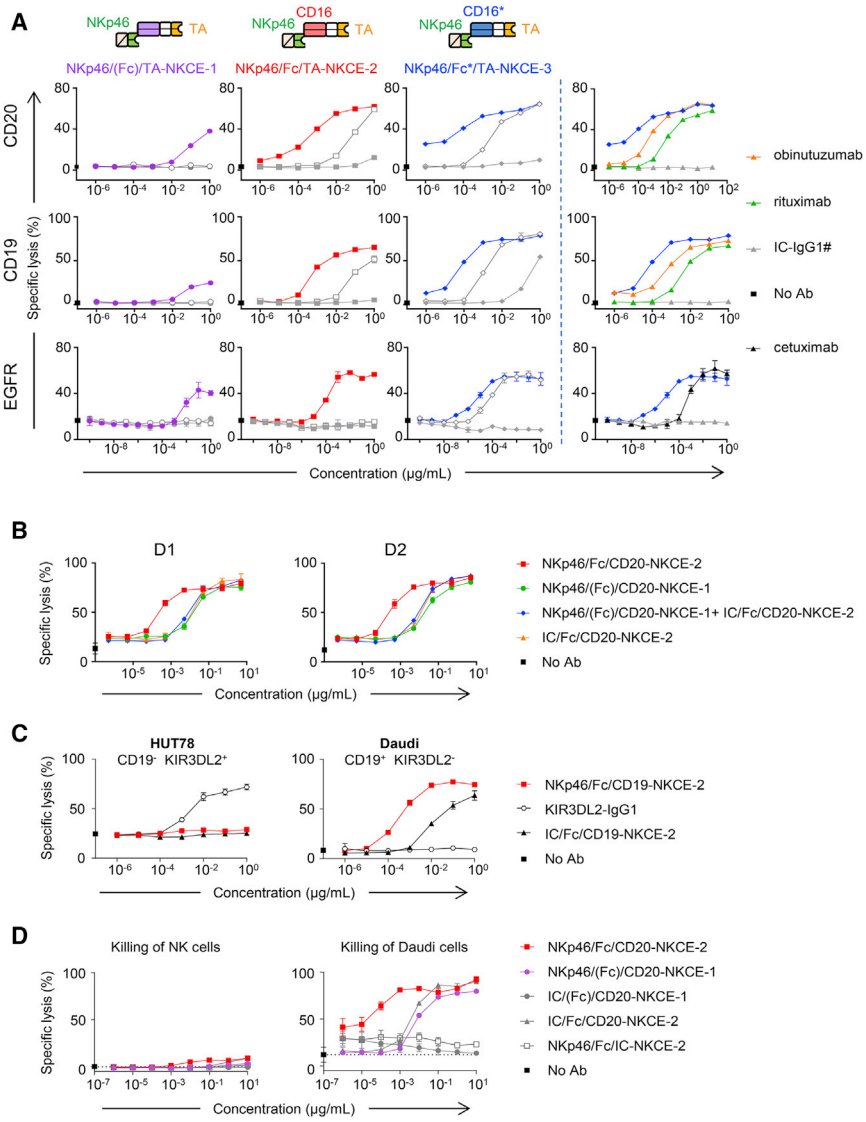

Figure 5. Trifunctional NKCEs Promoting ADCC Are More Efficient than Bispecific mAbs *In Vitro*

(A) Comparison of the cytotoxicities of NKp46 and NKp46-CD16 co-engagers to different TA and cell lines, with purified resting NK cells. For CD19 and CD20, Daudi B cell lymphoma cells were used as the target. For EGFR, the A549 lung adenocarcinoma cell line was used as the target (representative of n =10 experiments for CD19 and CD20 and n = 3 for EGFR). IgG1#: ADCC-enhanced IgG1.

(B) Comparison of the cytotoxicities of the NKCEs co-engaging CD16 and NKp46 (NKp46-1/Fc/CD20-NKCE-2) with a combination of molecules engaging NKp46 (NKp46-1/(FC)/CD20-NKCE-1) and CD16 (IC/Fc/CD20-NKCE-2) separately. Daudi cells were used as the target and purified resting NK cells as effectors. Results for two donors are shown.

(C) Cytotoxicities of NKp46-CD16 co-engagers in different cell lines expressing (Daudi B cell lymphoma, right panel) or not expressing (HUT78, cutaneous T cell lymphoma, left panel) the CD19 TA, with purified NK cells.

(D) Comparison of the cytotoxicities of NKp46 and NKp46-CD16 co-engagers targeting CD20 to purified resting NK cells and Daudi cells. Daudi cells were used as the target and purified resting NK cells (left panel) or Daudi cells (right panel) were loaded with ^{51}Cr to determine both Daudi-cell killing and NK-versus-NK toxicity in the same assay. Representative results from n = 2 experiments.

renal clear cell cancer is also associated with a favorable prognosis (Eckl et al., 2012; Habif et al., 2019; Remark et al., 2013). Conversely, NK-cell infiltration has no impact on clinical outcome in non-small-cell lung cancer, in which NK-cell cytotoxicity is impaired (Habif et al., 2019; Platonova et al., 2011). These findings support the importance of NK cells as immune effectors against tumors. One of the advantages of targeting NK cells rather than T cells in immunotherapy lies in the limited toxicity of NK-cell activation relative to that of T cells. An illustration of this difference between T and NK cells comes from the observation that the infusion of NK cells in patients is safer than the transfer of T cells, as NK cells do not induce graft-versus-host disease in allogeneic settings (Vivier et al., 2012).

We report here the development of a multispecific antibody technology for engaging NK cells. Trifunctional NKCEs targeting CD19, CD20, or EGFR as tumor antigens triggered tumor killing by human primary NK cells *in vitro*. *In vivo*, they induced NK-cell accumulation in tumors and promoted tumor clearance in preclinical mouse models of solid and invasive cancers. The approach used was based on innovative IgG-Fc multispecific antibody formats and first-in-class agonist anti-NKp46 mAbs activating NK cells only when cross-linked by tumor cells, with no off-target effects. CAR T cell therapies and bispecific T-cell engager treatments targeting T cells via the CD3 subunit of the T cell receptor are often associated with toxicity linked to the activation of a vast population of lymphocytes, as all T cells can be activated in these conditions. The advantage of targeting NK cells is that the frequency of NK cells is only ~10% that of T cells. Consequently, the risk of cytokine over production is expected to be lower. Unfortunately, mouse models are not predictive of the toxicity or immunogenicity of multispecific antibodies observed in humans, as observed for EpCAM-CD3 or CD20-CD3 BiTEs (Amann et al., 2008; Kebenko et al., 2018; Sun et al., 2015). However, our *in vitro* data are consistent with the absence of detectable toxicity linked to NKCEs, with efficacy superior to that of the best-in-class mAbs used in clinical practice, such as rituximab, obinutuzumab, and cetuximab.

Many T-cell-engager molecules are currently in clinical development, and most, including BiTEs, dual-affinity retargeting

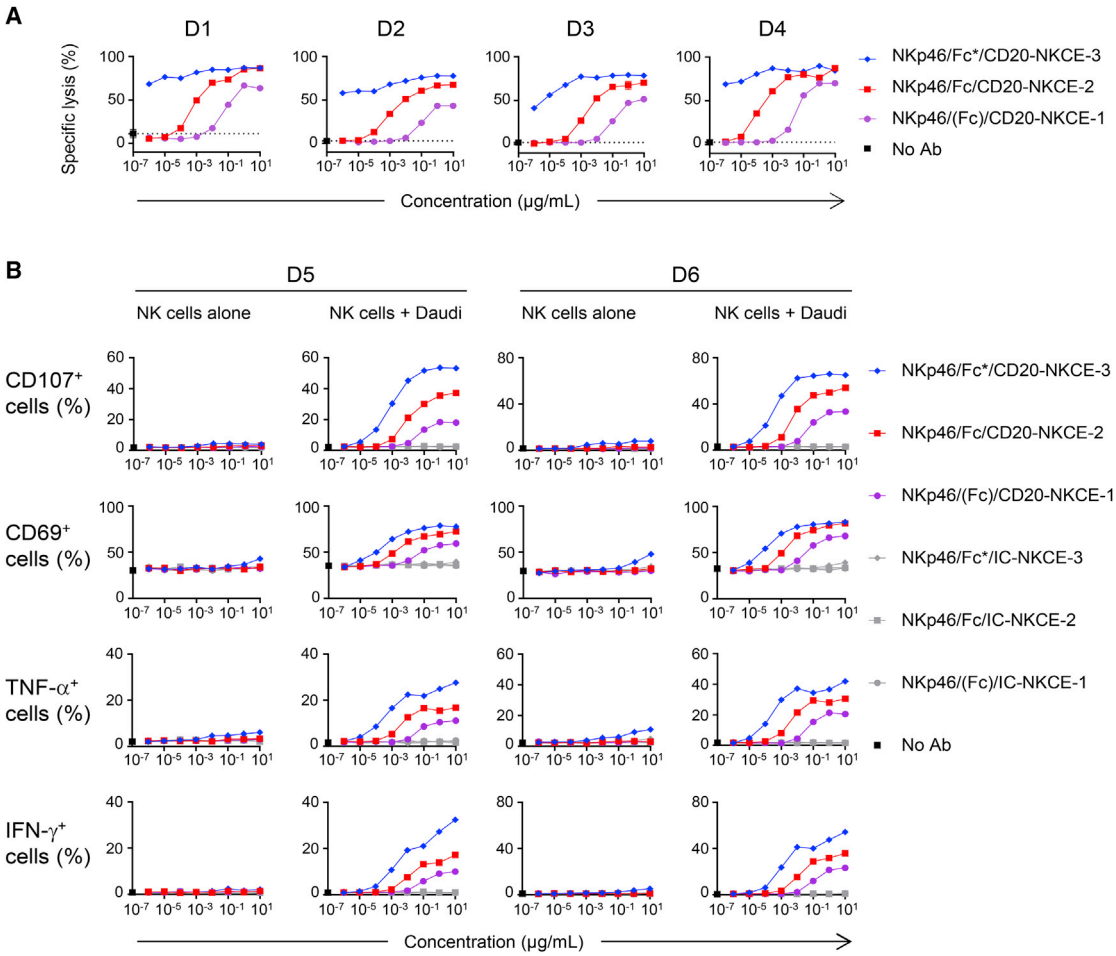

Figure 6. Trifunctional NKCEs Promoting NK-Cell Activation Are More Efficient than Bispecific mAbs *In Vitro*

(A) Comparison of the cytotoxicities of NKCEs harboring a silent, normal, or optimized Fc fragment against Daudi targets, with purified resting NK cells. Four donors are shown.

(B) Experiment similar to that in (A) but with the measurement, by flow cytometry, of CD107, CD69, TNF-α, and IFN-γ expression by NK cells. NK cells alone are compared with NK cells co-cultured with Daudi cells. Results for two donors are shown.

(DART) (Moore et al., 2011), and tandem diabody (TandAb) (Koch and Tesar, 2017), consist of scFv-like structures lacking an Fc domain and with a short half-life (2–7 h) in serum (Hoffman and Gore, 2014; Klinger et al., 2012). This short half-life may be beneficial in that it may limit toxic side effects, but it may also be associated with an inconvenient dosing regimen involving continuous infusions. New T-cell-engager formats harboring Fc fragments are now in clinical development, but little is known about the benefits of these molecules for patients, given their potential toxicity. NKCE formats open up new pharmacokinetic possibilities, with a long (>10 days) or short (<24 h) *in vivo* half-life. The lead multispecific NKCE formats (NKCE-2 and NKCE-3) were stable and had promising CMC profiles compatible with industrial development.

Other attempts to target NK cells in cancer immunotherapy have been described. Some have made use of the expression of NKG2D, but most have targeted CD16. The data reported here suggest that first-in-class anti-NKp46 mAbs were more potent activators of NK-cell effector functions than anti-NKG2D mAbs *in vitro*. The role of CD16-mediated ADCC may differ between indications and cancer stages, but studies have reported a correlation between CD16 polymorphism and the clinical efficacy of cetuximab and trastuzumab, a mAb targeting human epidermal growth factor receptor 2 (HER2) (Musolino et al., 2008; Rodríguez et al., 2012). CD16 polymorphism and affinity for Fcγ were also found to be correlated with clinical outcome in B cell lymphoma patients treated with anti-CD20 cytotoxic antibodies (Cartron et al., 2002; Weng and Levy, 2003). CD16 engagers are currently in clinical development, mostly for the treatment of hematological cancers (Davis et al., 2017; Rothe et al., 2015). BiKEs (bispecific killer cell engagers) engaging CD16 and TriKEs (trispecific killer cell engagers) engaging CD16 and containing an IL-15 moiety have also been developed to target antigens expressed on solid tumors, including EpCAM (Vallera et al., 2013), CD133 (Schmohl et al., 2017), or EpCAM and CD133 on several

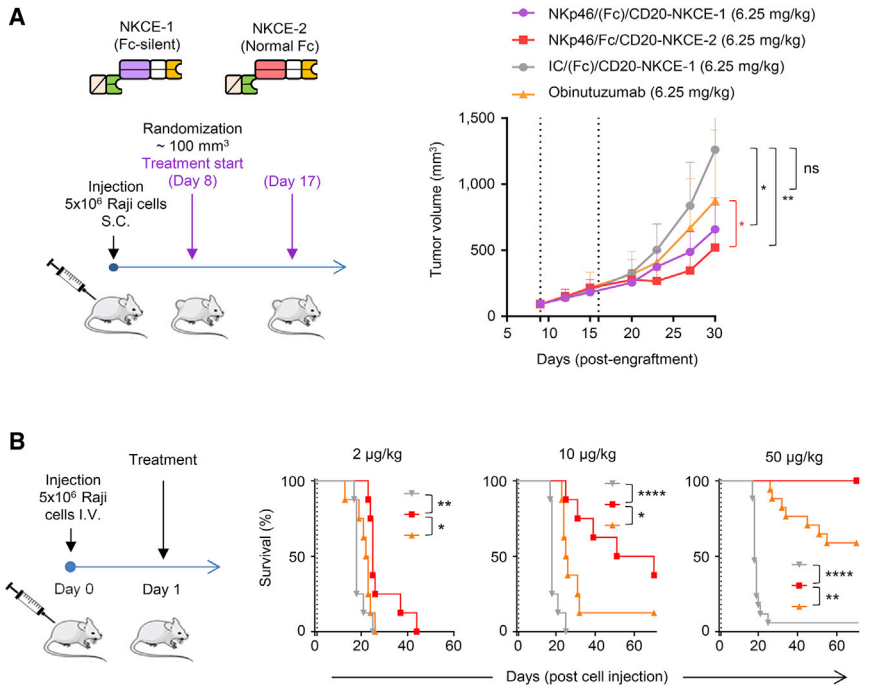

Figure 7. Trifunctional NKCEs Promoting ADCC Are More Efficient than Bispecific mAbs *In Vivo*

(A) Left panel: schematic diagram of the experimental setting. Right panel: Raji cells were s.c. injected into mice. Tumor-bearing mice were randomized to four groups (n = 10 for each group) treated once weekly for two weeks with 6.25 mg/kg body weight of IC/(Fc)/CD20-NKCE-1 (control group; gray), NKp46/(Fc)/CD20-NKCE-1 (purple), NKp46/Fc/CD20-NKCE-2 (red), or the anti-CD20 antibody obinutuzumab (orange). Mean tumor volumes ± SEM are shown. Mann-Whitney test *p < 0.05; **p < 0.01; n.s.: non-significant.

(B) Mice engrafted with Raji cells i.v. were treated on the day after cell injection with a range of doses of NKp46/Fc/CD20-NKCE-2 (red) or the anti-CD20 antibody obinutuzumab (orange). Kaplan-Meier curves were used to analyze mouse survival. Endpoint significance was calculated in a log-rank test. n = 8/group. *p < 0.05; **p < 0.01; ***p < 0.001; ****p < 0.0001.

cancers (Schmohl et al., 2016). The efficacy of both BiKEs and TriKEs was good both *in vitro* and in preclinical models. However, it remains unclear whether these multifunctional CD16 engager antibodies can activate tumor-infiltrating lymphocytes (TILs) expressing low levels of CD16 in solid tumors (Oberg et al., 2018). Our multispecific technology provides a versatile platform with different format options and the potential to co-engage up to three different activating receptors on NK cells and two different tumor antigens on cancer cells. With the trifunctional NKCEs reported here, the binding affinities for NKp46 (K_D=15 nM) and CD16 (K_D=1 µM and 29 nM for NKCE-2 and NKCE-3, respectively) should favor NK-cell targeting at the tumor bed, in which NKp46 expression levels remain high in many tumor conditions, in contrast to CD16, NKG2D, NKp30, and NKp44. As NKCEs have an affinity for NKp46 70 to 100 times stronger than that of the regular Fc for CD16, it is likely that NKCEs engage NKp46, before CD16, with no apparent steric hindrance. Trifunctional NKCEs should thus target NKp46$^+$ CD16$^+$ NK cells, rather than NKp46$^-$ CD16$^+$ myeloid cells and would also be able to activate NKp46$^+$ CD16^{low} NK TILs from tumor patients. Importantly, trifunctional NKCEs were found to be more potent than a mixture of the bispecific reagents activating NKp46 and CD16 separately. The co-targeting of NKp46 and CD16 thus led to full NK-cell activation, consistent with the findings of previous signaling studies (Bryceson et al., 2009). Together with the stronger anti-tumor activity of these molecules in preclinical models than of gold standard mAbs, such as rituximab, obinituzumab, and cetuximab, these results support the clinical development of NKCEs for cancer immunotherapy as a complement to existing immuno-oncology approaches.

STAR★METHODS

Detailed methods are provided in the online version of this paper and include the following:

- KEY RESOURCES TABLE
- CONTACT FOR REAGENT AND RESOURCE SHARING
- EXPERIMENTAL MODEL AND SUBJECT DETAILS
  - Mice
  - Cell lines
  - Human primary cells
- METHOD DETAILS
  - Immunohistochemistry
  - Human and cynomolgus recombinant protein production and purification
  - Production and purification of NKCEs
  - Production and purification of FcR
  - Epitope mapping
  - Surface plasmon resonance (SPR) experiments
  - Production and purification of antibodies
  - Titration of anti-NKp46 antibodies on human or cynomolgus NK cells
  - Assay of NK cell cytotoxicity to tumor cell lines
  - Activation of NK cells towards tumor cell lines
  - Mouse tissue preparation and flow cytometry analysis
  - *In vivo* murine tumor experiments
  - *In situ* hybridization
  - Image analysis
  - Protein production and purification for crystallization
  - Crystallization, data collection and processing
  - Structure determination

SUPPLEMENTAL INFORMATION

Supplemental Information can be found online at https://doi.org/10.1016/j.cell.2019.04.041.

A video abstract is available at https://doi.org/10.1016/j.cell.2019.04.041#mmc2.

ACKNOWLEDGMENTS

This article is dedicated to our late friend and colleague Pr. Alessandro Moretta, whose laboratory discovered NKp46 (Sivori et al., 1997) and who was a co-founder of Innate Pharma. We thank Sophie Ingoure (Innate Pharma), Jérémy Turchetto (Innate Pharma), Sabrina Carpentier (Innate Pharma), Ana Ines Lalanne (Institut Curie), Caroline Hoffmann (Institut Curie), and Olivier Lantz (Institut Curie) for help and advice during these studies. The project is supported by funding from the Fonds Européen de Dévelopement Régional (FEDER). The A.R. laboratory is supported by the French Infrastructure for Integrated Structural Biology (FRISBI) ANR-10-INBS-05. The E.V. laboratory is supported by funding from the European Research Council (ERC) under the European Union's Horizon 2020 research and innovation program (TILC, grant agreement No. 694502); the Agence Nationale de la Recherche including the PIONEER Project (ANR-17-RHUS-0007); Equipe Labellisée "La Ligue," Ligue Nationale contre le Cancer, MSDAvenir, Innate Pharma, and institutional grants to the CIML (INSERM, CNRS, and Aix-Marseille University) and to Marseille Immunopole.

AUTHOR CONTRIBUTIONS

L.G., F.R., and E.V. conceived the project. L.G., B.R., A.B.-A., A.M., N.A., S.C., R.R., and G.H. designed the experiments. L.G., B.R., S.C., H.R.-B., S.T., G.G., F.G., F.B., A.B.-A., M.S., B.A., F.C., S.A., and C.C. performed the experiments. A.R., Y.M., G.H., and R.R. analyzed the data. L.G., E.N.-M., and E.V. analyzed the data and wrote the manuscript with the help of the co-authors.

DECLARATION OF INTERESTS

L.G., A.M., N.A., B.R., A.B.-A., G.G., F.G., S.T., C.C., M.S., F.B., H.R.-B., S.C., G.H., S.A., R.R., Y.M., and E.V. are employees of Innate Pharma. L.G., A.M., N.A., and B.R. hold patents related to multifunctional antibodies engaging NK cells.

Received: December 5, 2018
Revised: March 19, 2019
Accepted: April 23, 2019
Published: May 30, 2019

REFERENCES

Amann, M., Brischwein, K., Lutterbuese, P., Parr, L., Petersen, L., Lorenczewski, G., Krinner, E., Bruckmeier, S., Lippold, S., Kischel, R., et al. (2008). Therapeutic window of MuS110, a single-chain antibody construct bispecific for murine EpCAM and murine CD3. Cancer Res. *68*, 143–151.

Baumeister, S.H., Freeman, G.J., Dranoff, G., and Sharpe, A.H. (2016). Coinhibitory Pathways in Immunotherapy for Cancer. Annu. Rev. Immunol. *34*, 539–573.

Blanc, E., Roversi, P., Vonrhein, C., Flensburg, C., Lea, S.M., and Bricogne, G. (2004). Refinement of severely incomplete structures with maximum likelihood in BUSTER-TNT. Acta Crystallogr. D Biol. Crystallogr. *60*, 2210–2221.

Brittenden, J., Heys, S.D., Ross, J., and Eremin, O. (1996). Natural killer cells and cancer. Cancer *77*, 1226–1243.

Bryceson, Y.T., March, M.E., Ljunggren, H.G., and Long, E.O. (2006). Activation, coactivation, and costimulation of resting human natural killer cells. Immunol. Rev. *214*, 73–91.

Bryceson, Y.T., Ljunggren, H.G., and Long, E.O. (2009). Minimal requirement for induction of natural cytotoxicity and intersection of activation signals by inhibitory receptors. Blood *114*, 2657–2666.

Cartron, G., Dacheux, L., Salles, G., Solal-Celigny, P., Bardos, P., Colombat, P., and Watier, H. (2002). Therapeutic activity of humanized anti-CD20 monoclonal antibody and polymorphism in IgG Fc receptor FcgammaRIIIa gene. Blood *99*, 754–758.

Cerwenka, A., and Lanier, L.L. (2018). Natural killers join the fight against cancer. Science *359*, 1460–1461.

Chen, D.S., and Mellman, I. (2017). Elements of cancer immunity and the cancer-immune set point. Nature *541*, 321–330.

Chiossone, L., Dumas, P.Y., Vienne, M., and Vivier, E. (2018). Natural killer cells and other innate lymphoid cells in cancer. Nat. Rev. Immunol. *18*, 671–688.

Clayton, A., Mitchell, J.P., Court, J., Linnane, S., Mason, M.D., and Tabi, Z. (2008). Human tumor-derived exosomes down-modulate NKG2D expression. J. Immunol. *180*, 7249–7258.

Crane, C.A., Han, S.J., Barry, J.J., Ahn, B.J., Lanier, L.L., and Parsa, A.T. (2010). TGF-beta downregulates the activating receptor NKG2D on NK cells and CD8+ T cells in glioma patients. Neuro-oncol. *12*, 7–13.

Davis, K.L., Agarwal, A.M., and Verma, A.R. (2017). Checkpoint inhibition in pediatric hematologic malignancies. Pediatr. Hematol. Oncol. *34*, 379–394.

Dennler, P., Chiotellis, A., Fischer, E., Brégeon, D., Belmant, C., Gauthier, L., Lhospice, F., Romagne, F., and Schibli, R. (2014). Transglutaminase-based chemo-enzymatic conjugation approach yields homogeneous antibody-drug conjugates. Bioconjug. Chem. *25*, 569–578.

Eckl, J., Buchner, A., Prinz, P.U., Riesenberg, R., Siegert, S.I., Kammerer, R., Nelson, P.J., and Noessner, E. (2012). Transcript signature predicts tissue NK cell content and defines renal cell carcinoma subgroups independent of TNM staging. J. Mol. Med. (Berl.) *90*, 55–66.

Emsley, P., and Cowtan, K. (2004). Coot: model-building tools for molecular graphics. Acta Crystallogr. D Biol. Crystallogr. *60*, 2126–2132.

Evans, P. (2006). Scaling and assessment of data quality. Acta Crystallogr. D Biol. Crystallogr. *62*, 72–82.

Fauriat, C., Just-Landi, S., Mallet, F., Arnoulet, C., Sainty, D., Olive, D., and Costello, R.T. (2007). Deficient expression of NCR in NK cells from acute myeloid leukemia: Evolution during leukemia treatment and impact of leukemia cells in NCRdull phenotype induction. Blood *109*, 323–330.

Foster, C.E., Colonna, M., and Sun, P.D. (2003). Crystal structure of the human natural killer (NK) cell activating receptor NKp46 reveals structural relationship to other leukocyte receptor complex immunoreceptors. J. Biol. Chem. *278*, 46081–46086.

Gauthier, L., and Rossi, B. (2016). Multispecific antigen binding proteins. US patent WO/2016/207273, filed April 22, 2016, and published October 27, 2016.

Glasner, A., Ghadially, H., Gur, C., Stanietsky, N., Tsukerman, P., Enk, J., and Mandelboim, O. (2012). Recognition and prevention of tumor metastasis by the NK receptor NKp46/NCR1. J. Immunol. *188*, 2509–2515.

Glasner, A., Levi, A., Enk, J., Isaacson, B., Viukov, S., Orlanski, S., Scope, A., Neuman, T., Enk, C.D., Hanna, J.H., et al. (2018). NKp46 Receptor-Mediated Interferon-gamma Production by Natural Killer Cells Increases Fibronectin 1 to Alter Tumor Architecture and Control Metastasis. Immunity *48*, 107–119.e4.

Guia, S., Fenis, A., Vivier, E., and Narni-Mancinelli, E. (2018). Activating and inhibitory receptors expressed on innate lymphoid cells. Semin. Immunopathol. *40*, 331–341.

Guillerey, C., and Smyth, M.J. (2016). NK Cells and Cancer Immunoediting. Curr. Top. Microbiol. Immunol. *395*, 115–145.

Habif, G., Crinier, A., André, P., Vivier, E., and Narni-Mancinelli, E. (2019). Targeting natural killer cells in solid tumors. Cell. Mol. Immunol. *16*, 415–422.

Halfteck, G.G., Elboim, M., Gur, C., Achdout, H., Ghadially, H., and Mandelboim, O. (2009). Enhanced in vivo growth of lymphoma tumors in the absence of the NK-activating receptor NKp46/NCR1. J. Immunol. *182*, 2221–2230.

Hoffman, L.M., and Gore, L. (2014). Blinatumomab, a Bi-Specific Anti-CD19/CD3 BiTE(®) Antibody for the Treatment of Acute Lymphoblastic Leukemia: Perspectives and Current Pediatric Applications. Front. Oncol. *4*, 63.

Imai, K., Matsuyama, S., Miyake, S., Suga, K., and Nakachi, K. (2000). Natural cytotoxic activity of peripheral-blood lymphocytes and cancer incidence: an 11-year follow-up study of a general population. Lancet *356*, 1795–1799.

June, C.H., O'Connor, R.S., Kawalekar, O.U., Ghassemi, S., and Milone, M.C. (2018). CAR T cell immunotherapy for human cancer. Science *359*, 1361–1365.

Kabsch, W. (2010). Integration, scaling, space-group assignment and post-refinement. Acta Crystallogr. D Biol. Crystallogr. *66*, 133–144.

Kebenko, M., Goebeler, M.E., Wolf, M., Hasenburg, A., Seggewiss-Bernhardt, R., Ritter, B., Rautenberg, B., Atanackovic, D., Kratzer, A., Rottman, J.B., et al. (2018). A multicenter phase 1 study of solitomab (MT110, AMG 110), a bispecific EpCAM/CD3 T-cell engager (BiTE®) antibody construct, in patients with refractory solid tumors. OncoImmunology *7*, e1450710.

Klinger, M., Brandl, C., Zugmaier, G., Hijazi, Y., Bargou, R.C., Topp, M.S., Gökbuget, N., Neumann, S., Goebeler, M., Viardot, A., et al. (2012). Immunopharmacologic response of patients with B-lineage acute lymphoblastic leukemia to continuous infusion of T cell-engaging CD19/CD3-bispecific BiTE antibody blinatumomab. Blood *119*, 6226–6233.

Koch, J., and Tesar, M. (2017). Recombinant Antibodies to Arm Cytotoxic Lymphocytes in Cancer Immunotherapy. Transfus. Med. Hemother. *44*, 337–350.

Lartigue, A., Gruez, A., Briand, L., Pernollet, J.C., Spinelli, S., Tegoni, M., and Cambillau, C. (2003). Optimization of crystals from nanodrops: crystallization and preliminary crystallographic study of a pheromone-binding protein from the honeybee Apis mellifera L. Acta Crystallogr. D Biol. Crystallogr. *59*, 919–921.

Mamessier, E., Sylvain, A., Thibult, M.L., Houvenaeghel, G., Jacquemier, J., Castellano, R., Gonçalves, A., André, P., Romagné, F., Thibault, G., et al. (2011). Human breast cancer cells enhance self tolerance by promoting evasion from NK cell antitumor immunity. J. Clin. Invest. *121*, 3609–3622.

Mandelboim, O., Lieberman, N., Lev, M., Paul, L., Arnon, T.I., Bushkin, Y., Davis, D.M., Strominger, J.L., Yewdell, J.W., and Porgador, A. (2001). Recognition of haemagglutinins on virus-infected cells by NKp46 activates lysis by human NK cells. Nature *409*, 1055–1060.

Mittal, D., Vijayan, D., and Smyth, M.J. (2018). Overcoming Acquired PD-1/PD-L1 Resistance with CD38 Blockade. Cancer Discov. *8*, 1066–1068.

Moore, P.A., Zhang, W., Rainey, G.J., Burke, S., Li, H., Huang, L., Gorlatov, S., Veri, M.C., Aggarwal, S., Yang, Y., et al. (2011). Application of dual affinity retargeting molecules to achieve optimal redirected T-cell killing of B-cell lymphoma. Blood *117*, 4542–4551.

Moretta, A., Bottino, C., Vitale, M., Pende, D., Biassoni, R., Mingari, M.C., and Moretta, L. (1996). Receptors for HLA class-I molecules in human natural killer cells. Annu. Rev. Immunol. *14*, 619–648.

Moretta, L., Bottino, C., Pende, D., Castriconi, R., Mingari, M.C., and Moretta, A. (2006). Surface NK receptors and their ligands on tumor cells. Semin. Immunol. *18*, 151–158.

Musolino, A., Naldi, N., Bortesi, B., Pezzuolo, D., Capelletti, M., Missale, G., Laccabue, D., Zerbini, A., Camisa, R., Bisagni, G., et al. (2008). Immunoglobulin G fragment C receptor polymorphisms and clinical efficacy of trastuzumab-based therapy in patients with HER-2/neu-positive metastatic breast cancer. J. Clin. Oncol. *26*, 1789–1796.

Narni-Mancinelli, E., Gauthier, L., Baratin, M., Guia, S., Fenis, A., Deghmane, A.E., Rossi, B., Fourquet, P., Escalière, B., Kerdiles, Y.M., et al. (2017). Complement factor P is a ligand for the natural killer cell-activating receptor NKp46. Sci. Immunol. *2*, eaam9628.

Oberg, H.H., Kellner, C., Gonnermann, D., Sebens, S., Bauerschlag, D., Gramatzki, M., Kabelitz, D., Peipp, M., and Wesch, D. (2018). Tribody [(HER2)$_2$xCD16] Is More Effective Than Trastuzumab in Enhancing γδ T Cell and Natural Killer Cell Cytotoxicity Against HER2-Expressing Cancer Cells. Front. Immunol. *9*, 814.

Okazaki, T., and Honjo, T. (2007). PD-1 and PD-1 ligands: from discovery to clinical application. Int. Immunol. *19*, 813–824.

Okazaki, T., Chikuma, S., Iwai, Y., Fagarasan, S., and Honjo, T. (2013). A rheostat for immune responses: the unique properties of PD-1 and their advantages for clinical application. Nat. Immunol. *14*, 1212–1218.

Pessino, A., Sivori, S., Bottino, C., Malaspina, A., Morelli, L., Moretta, L., Biassoni, R., and Moretta, A. (1998). Molecular cloning of NKp46: a novel member of the immunoglobulin superfamily involved in triggering of natural cytotoxicity. J. Exp. Med. *188*, 953–960.

Platonova, S., Cherfils-Vicini, J., Damotte, D., Crozet, L., Vieillard, V., Validire, P., André, P., Dieu-Nosjean, M.C., Alifano, M., Régnard, J.F., et al. (2011). Profound coordinated alterations of intratumoral NK cell phenotype and function in lung carcinoma. Cancer Res. *71*, 5412–5422.

Ponassi, M., Cantoni, C., Biassoni, R., Conte, R., Spallarossa, A., Pesce, A., Moretta, A., Moretta, L., Bolognesi, M., and Bordo, D. (2003). Structure of the human NK cell triggering receptor NKp46 ectodomain. Biochem. Biophys. Res. Commun. *309*, 317–323.

Pross, H.F., and Lotzová, E. (1993). Role of natural killer cells in cancer. Nat. Immun. *12*, 279–292.

Rautela, J., Souza-Fonseca-Guimaraes, F., Hediyeh-Zadeh, S., Delconte, R.B., Davis, M.J., and Huntington, N.D. (2018). Molecular insight into targeting the NK cell immune response to cancer. Immunol. Cell Biol. *96*, 477–484.

Remark, R., Alifano, M., Cremer, I., Lupo, A., Dieu-Nosjean, M.C., Riquet, M., Crozet, L., Ouakrim, H., Goc, J., Cazes, A., et al. (2013). Characteristics and clinical impacts of the immune environments in colorectal and renal cell carcinoma lung metastases: influence of tumor origin. Clin. Cancer Res. *19*, 4079–4091.

Rodríguez, J., Zarate, R., Bandres, E., Boni, V., Hernández, A., Sola, J.J., Honorato, B., Bitarte, N., and García-Foncillas, J. (2012). Fc gamma receptor polymorphisms as predictive markers of Cetuximab efficacy in epidermal growth factor receptor downstream-mutated metastatic colorectal cancer. Eur. J. Cancer *48*, 1774–1780.

Rothe, A., Sasse, S., Topp, M.S., Eichenauer, D.A., Hummel, H., Reiners, K.S., Dietlein, M., Kuhnert, G., Kessler, J., Buerkle, C., et al. (2015). A phase 1 study of the bispecific anti-CD30/CD16A antibody construct AFM13 in patients with relapsed or refractory Hodgkin lymphoma. Blood *125*, 4024–4031.

Saito, H., Osaki, T., and Ikeguchi, M. (2012). Decreased NKG2D expression on NK cells correlates with impaired NK cell function in patients with gastric cancer. Gastric Cancer *15*, 27–33.

Schantz, S.P., and Ordonez, N.G. (1991). Quantitation of natural killer cell function and risk of metastatic poorly differentiated head and neck cancer. Nat. Immun. Cell Growth Regul. *10*, 278–288.

Schantz, S.P., Campbell, B.H., and Guillamondegui, O.M. (1986). Pharyngeal carcinoma and natural killer cell activity. Am. J. Surg. *152*, 467–474.

Schantz, S.P., Savage, H.E., Racz, T., Taylor, D.L., and Sacks, P.G. (1989). Natural killer cells and metastases from pharyngeal carcinoma. Am. J. Surg. *158*, 361–366.

Schmohl, J.U., Felices, M., Todhunter, D., Taras, E., Miller, J.S., and Vallera, D.A. (2016). Tetraspecific scFv construct provides NK cell mediated ADCC and self-sustaining stimuli via insertion of IL-15 as a cross-linker. Oncotarget *7*, 73830–73844.

Schmohl, J.U., Felices, M., Oh, F., Lenvik, A.J., Lebeau, A.M., Panyam, J., Miller, J.S., and Vallera, D.A. (2017). Engineering of Anti-CD133 Trispecific Molecule Capable of Inducing NK Expansion and Driving Antibody-Dependent Cell-Mediated Cytotoxicity. Cancer Res. Treat. *49*, 1140–1152.

Schumacher, T.N., and Schreiber, R.D. (2015). Neoantigens in cancer immunotherapy. Science *348*, 69–74.

Sharma, P., and Allison, J.P. (2015). Immune checkpoint targeting in cancer therapy: toward combination strategies with curative potential. Cell *161*, 205–214.

Shields, M.A., Dangi-Garimella, S., Krantz, S.B., Bentrem, D.J., and Munshi, H.G. (2011). Pancreatic cancer cells respond to type I collagen by inducing snail expression to promote membrane type 1 matrix metalloproteinase-dependent collagen invasion. J. Biol. Chem. *286*, 10495–10504.

Sivori, S., Vitale, M., Morelli, L., Sanseverino, L., Augugliaro, R., Bottino, C., Moretta, L., and Moretta, A. (1997). p46, a novel natural killer cell-specific surface molecule that mediates cell activation. J. Exp. Med. *186*, 1129–1136.

Sivori, S., Pende, D., Bottino, C., Marcenaro, E., Pessino, A., Biassoni, R., Moretta, L., and Moretta, A. (1999). NKp46 is the major triggering receptor involved in the natural cytotoxicity of fresh or cultured human NK cells. Correlation between surface density of NKp46 and natural cytotoxicity against autologous, allogeneic or xenogeneic target cells. Eur. J. Immunol. *29*, 1656–1666.

Slaney, C.Y., Wang, P., Darcy, P.K., and Kershaw, M.H. (2018). CARs versus BiTEs: A Comparison between T Cell-Redirection Strategies for Cancer Treatment. Cancer Discov. *8*, 924–934.

Smyth, M.J., Thia, K.Y., Street, S.E., Cretney, E., Trapani, J.A., Taniguchi, M., Kawano, T., Pelikan, S.B., Crowe, N.Y., and Godfrey, D.I. (2000a). Differential tumor surveillance by natural killer (NK) and NKT cells. J. Exp. Med. *191*, 661–668.

Smyth, M.J., Thia, K.Y., Street, S.E., MacGregor, D., Godfrey, D.I., and Trapani, J.A. (2000b). Perforin-mediated cytotoxicity is critical for surveillance of spontaneous lymphoma. J. Exp. Med. *192*, 755–760.

Smyth, M.J., Crowe, N.Y., and Godfrey, D.I. (2001). NK cells and NKT cells collaborate in host protection from methylcholanthrene-induced fibrosarcoma. Int. Immunol. *13*, 459–463.

Spiess, C., Zhai, Q., and Carter, P.J. (2015). Alternative molecular formats and therapeutic applications for bispecific antibodies. Mol. Immunol. *67* (2 Pt A), 95–106.

Street, S.E., Zerafa, N., Iezzi, M., Westwood, J.A., Stagg, J., Musiani, P., and Smyth, M.J. (2007). Host perforin reduces tumor number but does not increase survival in oncogene-driven mammary adenocarcinoma. Cancer Res. *67*, 5454–5460.

Sun, L.L., Ellerman, D., Mathieu, M., Hristopoulos, M., Chen, X., Li, Y., Yan, X., Clark, R., Reyes, A., Stefanich, E., et al. (2015). Anti-CD20/CD3 T cell-dependent bispecific antibody for the treatment of B cell malignancies. Sci. Transl. Med. *7*, 287ra70.

Trinchieri, G. (1989). Biology of natural killer cells. Adv. Immunol. *47*, 187–376.

Vagin, A., and Teplyakov, A. (2010). Molecular replacement with MOLREP. Acta Crystallogr. D Biol. Crystallogr. *66*, 22–25.

Vallera, D.A., Zhang, B., Gleason, M.K., Oh, S., Weiner, L.M., Kaufman, D.S., McCullar, V., Miller, J.S., and Verneris, M.R. (2013). Heterodimeric bispecific single-chain variable-fragment antibodies against EpCAM and CD16 induce effective antibody-dependent cellular cytotoxicity against human carcinoma cells. Cancer Biother. Radiopharm. *28*, 274–282.

Vivier, E., Ugolini, S., Blaise, D., Chabannon, C., and Brossay, L. (2012). Targeting natural killer cells and natural killer T cells in cancer. Nat. Rev. Immunol. *12*, 239–252.

Vivier, E., Artis, D., Colonna, M., Diefenbach, A., Di Santo, J.P., Eberl, G., Koyasu, S., Locksley, R.M., McKenzie, A.N.J., Mebius, R.E., et al. (2018). Innate Lymphoid Cells: 10 Years On. Cell *174*, 1054–1066.

Walzer, T., Bléry, M., Chaix, J., Fuseri, N., Chasson, L., Robbins, S.H., Jaeger, S., André, P., Gauthier, L., Daniel, L., et al. (2007). Identification, activation, and selective in vivo ablation of mouse NK cells via NKp46. Proc. Natl. Acad. Sci. USA *104*, 3384–3389.

Wang, H., Yang, D., Xu, W., Wang, Y., Ruan, Z., Zhao, T., Han, J., and Wu, Y. (2008). Tumor-derived soluble MICs impair CD3(+)CD56(+) NKT-like cell cytotoxicity in cancer patients. Immunol. Lett. *120*, 65–71.

Weng, W.K., and Levy, R. (2003). Two immunoglobulin G fragment C receptor polymorphisms independently predict response to rituximab in patients with follicular lymphoma. J. Clin. Oncol. *21*, 3940–3947.

Winn, M.D., Ballard, C.C., Cowtan, K.D., Dodson, E.J., Emsley, P., Evans, P.R., Keegan, R.M., Krissinel, E.B., Leslie, A.G., McCoy, A., et al. (2011). Overview of the CCP4 suite and current developments. Acta Crystallogr. D Biol. Crystallogr. *67*, 235–242.

Wolf, E., Hofmeister, R., Kufer, P., Schlereth, B., and Baeuerle, P.A. (2005). BiTEs: bispecific antibody constructs with unique anti-tumor activity. Drug Discov. Today *10*, 1237–1244.

Wu, N., and Veillette, A. (2016). SLAM family receptors in normal immunity and immune pathologies. Curr. Opin. Immunol. *38*, 45–51.

Wu, J.D., Higgins, L.M., Steinle, A., Cosman, D., Haugk, K., and Plymate, S.R. (2004). Prevalent expression of the immunostimulatory MHC class I chain-related molecule is counteracted by shedding in prostate cancer. J. Clin. Invest. *114*, 560–568.

Ying, T., Chen, W., Gong, R., Feng, Y., and Dimitrov, D.S. (2012). Soluble monomeric IgG1 Fc. J. Biol. Chem. *287*, 19399–19408.

STAR★METHODS

KEY RESOURCES TABLE

REAGENT or RESOURCE	SOURCE	IDENTIFIER
Antibodies		
Ultra-LEAF purified anti-Asialo GM1 (Poly 21460)	BioLegend	Cat# 146002; RRID: AB_2562206
Anti-NKp46 (clone 8E5B)	Innate Pharma	N/A
Rituximab	Roche	MabThera/Rituxan
Obinutuzumab	Roche	Gazyva/Gazyvaro
Cetuximab	Merck	Erbitux
Anti-CD56-PEVio770	Miltenyi	Cat# 130-100-676; RRID: AB_2658738
Anti-NKp46-PE	Beckman Coulter	Cat# IM3711; RRID: AB_1575960
Anti-NKG2D-PE	Beckman Coulter	Cat# A08934
Anti-NKp46-1-PE	Innate Pharma	N/A
Anti-CD14-FITC (cynomolgus)	Becton Dickinson	Cat# 555397; RRID: AB_395798
Anti-CD3-Pacific Blue (cynomolgus and human)	Becton Dickinson	Cat# 558124; RRID: AB_397044
Anti-CD20-PerCP (cynomolgus)	Miltenyi Biotec	Cat# 130-113-376; RRID: AB_2726144
Anti-NKG2A-APC (cynomolgus)	Beckman Coulter	Cat# A60797; RRID: AB_10643105
Anti-CD69-PE	Miltenyi Biotec	Cat# 130-092-160; RRID: AB_615102
Anti-CD107a-APC	Becton Dickinson	Cat# 641581; RRID: AB_1645722
Anti-CD107a-APC	Miltenyi	Cat# 130-095-510
Anti-CD107b-eFluor660	eBioscience	Cat# 50-1078-42
Anti-CD107b-APC	Miltenyi	Cat# 130-103-960
Anti-TNF-BUV395	Becton Dickinson	Cat# 563996
Anti-IFNγ-BV605	Biolegend	Cat# 502536
Goat anti-human IgG (Fc)-PE	Jackson Immunoresearch	Cat# 109-116-170; RRID: AB_2337681
Goat anti-mouse PE Fcγ specific	Jackson Immunoresearch	Cat# 115-116-071
Anti-CD45 APC, mouse (30-F11)	Becton Dickinson	Cat# 559864; RRID: AB_398672
Anti-NKp46 VioBlue, mouse (29A1.4)	Miltenyi Biotec	Cat# 130-102-185; RRID: AB_2661351
Anti-CD3 FITC, mouse (145-2C11)	Becton Dickinson	Cat# 553062; RRID: AB_394595
Optilyse C	Beckman Coulter	Cat# A11895
Anti-CD45 APC R700, mouse (30-F11)	Becton Dickinson	Cat# 565478
Anti-CD11b BUV737, mouse (M1/70)	Becton Dickinson	Cat# 564443
Anti-Gr1 BUV395, mouse (RB6-8C5)	Becton Dickinson	Cat# 563849
Anti-Ly-6C FITC, mouse (AL-21)	Becton Dickinson	Cat# 553104; RRID: AB_394628
Anti-NKp46 BV421, mouse (29A1.4)	Becton Dickinson	Cat# 562850
Anti-CD11c PE, mouse (HL3)	Becton Dickinson	Cat# 557401; RRID: AB_396684
Anti-CD45 eFluor450, mouse (30-F11)	eBioscience	Cat# 48-0451-82; RRID: AB_1518806
Anti-Ly-6G PerCPCy5.5, mouse (1A8)	Becton Dickinson	Cat# 560602; RRID: AB_1727563
Anti-CD11b V500, mouse (M1/70)	Becton Dickinson	Cat# 562127
Anti-F4/80 APCeFluor780, mouse (BM8)	eBioscience	Cat# 47-4801-82; RRID: AB_2735036
ultraView Universal DAB Detection Kit	Roche	RRID: AB_2753116
RNAscope 2.5 LS probe DapB		Cat# 312038
RNAscope 2.5 LS probe Mm-PPIB		Cat# 313918
RNAscope 2.5 LS probe Mm-Ncr1		Cat# 501728
LumaPlate-96	Perkin Elmer	Cat# 6006633
Sensor Chip C1	GE healthcare	Cat# BR100540

(*Continued on next page*)

Continued

REAGENT or RESOURCE	SOURCE	IDENTIFIER
Cell preparation tube	BD Vacutainer®	Cat# 362782
Pure yield plasmid midiprep	Promega	Cat# A2495
NucleoSpin 96 plasmid	Macherey-Nagel	Cat# 740625.4
Ni-NTA beads	Qiagen	Cat# 1018244
rProtein A Fast Flow	GE Healthcare	Cat# 17-1279-03
Superdex 200 increase 10/300 GL	GE Healthcare	Cat# 28-9909-44
HiTrap SP HP column 1mL	GE Healthcare	Cat# 17-1151-01
Goat anti-human IgG-Alexa488	Jackson Immunoresearch	Cat# 109-546-088
Matrigel Basement Membrane Matrix	Corning	Cat# 354234
Normal rabbit serum	Abcam	Cat# Ab7487
BD CellFIX	Becton Dickinson	Cat# 340181
BD Cytofix/Cytoperm	Becton Dickinson	Cat# 554722
BD Perm/Wash	Becton Dickinson	Cat# 554723
*Hin*dIII restriction enzyme	Thermo Fisher Scientific	Cat# FD0504
*Xba*I restriction enzyme	Thermo Fisher Scientific	Cat# FD0684
Dulbecco's phosphate-buffered saline (DPBS)	Gibco	Cat# 14190-094
DMEM	Gibco	Cat# 41965-039
PEI max	Polysciences Inc	Cat# 24765
EXPI293 expression medium	Gibco	Cat# A14351-01
Valproic acid sodium salt	Sigma	Cat# P4543-10G
D(+) glucose monohydrate	Fluka	Cat# 49161
Tryptone N1	Organo Technie	Cat# 19553
Instant Blue	Expedeon	ISB1L
Polyethylene glycol 1500	Sigma Aldrich	Cat# 25322-68-3
MMT buffer:DL-Malic acid, MES monohydrate, Tris: pH 4.0-9.0	Molecular dimension	Cat# 6915-15-7, 4432-31-9, 77-86-1
Poly(ethylene glycol) methyl ether 500	Molecular dimension	Cat# 9004-74-4
Poly(ethylene glycol) 20000	Molecular dimension	Cat# 25322-68-3
Trizma base	Molecular dimension	Cat# 77-86-1
BICINE	Molecular dimension	Cat# 150-25-4
Chromium-51 radionuclide	Perkin Elmer	NEZ030002MC
Glutamax	Gibco	Cat# 35050-038
Triton X-100	Sigma Aldrich	Cat# 93443
hIL-2	Miltenyi Biotec	Cat# 130-097-748
Bovine serum albumin (BSA)	Sigma Aldrich	Cat# A9418
EDTA	Invitrogen	Cat# 15575-038
Sodium azide	Sigma Aldrich	Cat# 71290
Ficoll Paque Plus	GE healthcare	Cat# 17-1440-03
RPMI 1640 medium	GIBCO	Cat# 31870-025
Fetal bovine serum (FBS)	GIBCO	Cat# 10270-106
L-glutamine	GIBCO	Cat# 25030-024
Lipofectamine 2000	ThermoFisher Scientific	Cat# 11668027
Non-essential amino acids solution (NEAA)	GIBCO	Cat# 11140-035
Ammonium chloride solution	Stemcell	Cat# 07800
NK Cell Isolation Kit, human	MACS Miltenyi Biotec	Cat# 130-092-657
LIVE/DEAD Fixable Near-IR Dead Cell Stain Kit	Molecular Probes	Cat# L34976
LIVE/DEAD Fixable Red Dead Cell Stain Kit	Molecular Probes	Cat# L34972
LIVE/DEAD Fixable BlueDead Cell Stain Kit	Molecular Probes	Cat# L34962

(*Continued on next page*)

Continued

REAGENT or RESOURCE	SOURCE	IDENTIFIER
LIVE/DEAD Fixable Aqua Dead Cell Stain Kit	Molecular Probes	Cat# L34966
PCR Clean-up gel extraction kit	Macherey-Nagel	Cat# 740609
Endotoxin kit	Charles Rivers	Cat# R1708K
In-Fusion system	Clontech	Cat# 639644
Experimental Models: Cell Lines		
Raji	ATCC	CCL-86; CVCL 0511
Daudi	DSMZ	ACC-78
HUT78	ATCC (LGC Standards)	TIB-161
KHYG-1	JCRB cell bank	JCRB0156
EXPI-293F	ThermoFisher Scientific	#A14527
A549	ATCC	CCL-185; CVCL 0023
CB-17 SCID	Janvier Laboratories	CB-17/Icr-Prkdcscid/scid/Rj; MGI: 2160375
Human whole blood	EFS Marseille	N/A
Cynomolgus whole blood	CNRS Marseille	N/A
Oligonucleotides		
ECD huNKp46 Forward 5′ TACGACTCACAAGCTTGCCGCCACCATGT CTTCCACACTCCCTGC 3′		N/A
ECD huNKp46 Reverse 5′ CCGCCCCGACTCTA GATCAATGGTGATGGTGGTGATGATTCTGGG CAGTGTGATCCC 3′		N/A
ECD cyNKp46 Forward 5′ TACGACTCACAAGCTTGCCGCCACCATGT CTTCCACACTCCGTGC 3′		N/A
ECD cyNKp46 Reverse 5′ CCGCCCCGACTCTAGATCAGTGATGGTGA TGGTGATGATTCTGGGCAGTGTGGTCC 3′		N/A
SLX192 vector	Selexis	N/A
pTT-5 vector	CNCR	N/A

CONTACT FOR REAGENT AND RESOURCE SHARING

Further information and requests for resources and reagents should be addressed to the Lead Contact, Eric Vivier (vivier@ciml.univ-mrs.fr).

EXPERIMENTAL MODEL AND SUBJECT DETAILS

Mice

CB-17 severe combined immune-deficient (SCID) mice reared at Janvier Laboratories under specific pathogen-free conditions were used. Female mice were used at eight to 10 weeks of age and were allowed to acclimate to the housing facility for at least one week. All animal experiments were performed in accordance with the rules of the Innate Pharma ethics and animal welfare committees.

Cell lines

The Raji and Daudi human Burkitt B-cell lymphoma lines (ATCC CCL-86 and DSMZ ACC-78 respectively), the HUT78 Sézary syndrome cell line (ATCC (LGC Standards) TIB-161), the KHYG-1 human NK cell leukemia line (JCRB cell bank JCRB0156) and the A549 human lung carcinoma cell line (ATCC CCL-185) were cultured in RPMI 1640 medium (Gibco) supplemented with 10% heat-inactivated fetal bovine serum (FBS, Gibco), 2 mM L-glutamine (Gibco), 1% non-essential amino acids (Gibco) and 1 mM sodium pyruvate (Gibco) and maintained at 37°C under an atmosphere containing 5% CO_2. We added 200 IU/mL hIL-2 (Miltenyi Biotec) to the KHYG-1 cell culture medium.

Human primary cells

Peripheral blood samples from healthy donors were obtained from *Etablissement Francais du Sang* (EFS, Marseille) with written consent obtained from each volunteer. Peripheral blood, metastatic and non-metastatic lymph node, tumor and tumor-adjacent tissues from cancer patients were obtained at the time of surgical resection according to a protocol approved by Institut Curie, with written informed consent from each patient.

Peripheral blood samples from cynomolgus monkeys (*Macaca fascicularis*) were obtained from the Centre National de la Recherche Scientifique (CNRS, Marseille).

METHOD DETAILS

Immunohistochemistry

Commercially available formalin-fixed paraffin-embedded (FFPE) tumor tissue microarrays (lung (#LC10012a), pancreas (#PA1001b), stomach (#ST1003a), kidney (#HKid-CRCC150CS-02), colon (#BC051110b), head and neck (#HN802b) and liver (#BC03119a); all from US Biomax) were stained on a Benchmark stainer (Ventana). After pretreatment with cell conditioning 1 solution (Ventana), sections were incubated for 1 hour at 37°C with an anti-NKp46 Ab (clone 8E5B, Innate Pharma) at a concentration of 5 μg/mL or for 2 hours at 37°C with an anti-CD8 Ab (clone C8/144B, Dako) at a concentration of 3 μg/mL. An anti-mouse/rabbit IgG detection system (Ultraview universal DAB detection kit, Ventana) was used for primary Ab detection and amplification. Tissues were counterstained with hematoxylin II and then washed, dehydrated, cleared and mounted with a coverslipper (ClearVue, Thermo Fisher Scientific). Slides were scanned on a Nanozoomer 2.0-HT slide scanner (Hamamatsu). Positive and negative controls (FFPE cell pellets) were included in each run.

Human and cynomolgus recombinant protein production and purification

The sequence encoding the ECD of human NKp46 (Gln22-Asn255, NM_004829.5) was inserted into the SLX192 vector between the *Hin*dIII and *Xba*I restriction sites. A C-terminal 6xHis tag was added for purification. The following primers were used for PCR on human PBMCs: 5′ TACGACTCACAAGCTTGCCGCCACCATGTCTTCCACACTCCCTGC 3′ and 5′ CCGCCCCGACTCTAGATCAA TGGTGATGGTGGTGATGATTCTGGGCAGTGTGATCCC 3′. The sequence of the amplicon was checked. The vector was then used to transfect a CHO cell line and a clone producing the protein was selected. The protein was purified from the culture supernatant with Ni-NTA beads (Qiagen, #1018244) and S200 size exclusion chromatography was performed to ensure the elimination of aggregates. The same protocol was used to clone and produce the ECD of the cynomolgus monkey NKp46 (Gln17-Asn254; NP_001271509.1). The primers used to amplify the expected sequence from cynomolgus monkey PBMCs were: 5′ TACGACTCACAAGCTTGCCGCCACCATGTCTTCCACACTCCGTGC 3′ and 5′ CCGCCCCGACTCTAGATCAGTGATGGT GATGGTGATGATTCTGGGCAGTGTGGTCC 3′.

Production and purification of NKCEs

The sequences encoding the different fragments of each bispecific molecule were inserted into the pTT-5 vector between the *Hin*dIII and *Bam*HI restriction sites. Expression vectors (prepared as endotoxin-free midipreps) were used to cotransfect EXPI-293F cells (Life Technologies) in the presence of PEI (37°C, 5% CO_2, 150 rpm). The cells were used to seed culture flasks at a density of 1 x 10^6 cells per ml and cultured in EXPI293 medium (Gibco) supplemented with valproic acid (final concentration 0.5 mM), glucose (4 g/L) and tryptone N1 (0.5%). The supernatant was harvested after six days and passed through a Stericup filter with 0.22 μm pores. NKCES were purified with Protein A beads (250 μl/50 ml SN), eluted with 0.1 M sodium citrate buffer at pH 3 and immediately neutralized with 1 M Tris pH 8. The proteins were then dialyzed overnight with 1 x PBS at 4°C and concentrated to 10 mg/ml before loading on an S200 Increase 10/300 column (AKTA, 500 μl injection loop). The proteins yielding a peak at the expected size were harvested and analyzed by analytical SEC and SDS-PAGE under reducing and non-reducing conditions, with Coomassie brilliant blue staining. Alternatively, NKCEs were dialyzed against 50 mM MES buffer pH 6.2 and purified by ion-exchange chromatography on a 1 mL SP-HP column (GE Healthcare). All the purified molecules were stored in 1 x PBS and analyzed to check for the absence of aggregates and endotoxins.

Production and purification of FcR

The ECDs of human FcγRI (CD64), human FcγRIIa (CD32a), human FcγRIIb (CD32b), FcγRIIIa (CD16aV), FcγRIIIa (CD16aF) and FcγRIIIb (CD16b) were inserted into the SLX192 vector between the *Hin*dIII and *Xba*I restriction sites. The sequences of the inserts were checked. Each vector was then used to transfect CHO cells, and producer sub-clones were then selected for each molecule. FcRs were purified from the culture supernatants of the CHO clones with NiNTA agarose beads (Qiagen). Proteins were eluted with an imidazole gradient and dialyzed against 1 x PBS. Protein quality was checked by SDS-PAGE and analytical size exclusion chromatography, and for the absence of endotoxins.

Epitope mapping

NKp46 mutants were designed for epitope mapping by flow cytometry for the various antibodies. The mutants were defined on the basis of one, two or three substitutions of amino acids exposed at the molecular surface over the two ECDs of NKp46. This approach

led to the design of 36 mutants, described in Table S1. Residues were numbered as in a previous article (Foster et al., 2003). The NKp46 mutants were generated by PCR. The amplicons were subjected to electrophoresis in agarose gels and purified with the Macherey Nagel PCR Clean-Up Gel Extraction kit. The two or three purified PCR products generated for each mutant were then ligated into an SLX192 vector (digested with the restriction enzymes *Hin*dIII and *XBa*I), with the ClonTech InFusion system, according to the manufacturer's instructions. The vectors containing the mutated sequences were prepared as minipreps and sent to MWG-Biotech for sequencing. The vectors containing the mutated sequences were then prepared as midipreps with the Promega PureYield™ Plasmid Midiprep System. They were then used to transfect the HEK-293T cell line grown in DMEM (Invitrogen) supplemented with 2 mM GlutaMax, sodium pyruvate and 10% heat-inactivated fetal calf serum (Thermo Fisher Scientific). The cells were grown in static conditions at 37°C, under an atmosphere containing 10% CO_2. We used $6x10^5$ cells to seed a T75 flask the day before transfection. These cells were cotransfected with an NKp46 mutant vector (20 μg) and the DAP-12 vector (20 μg), in the presence of Lipofectamine 2000 (Invitrogen), according to the manufacturer's instructions. All the anti-NKp46 antibodies were tested for binding to each mutant at a concentration of 10 μg/mL or by titration (1 – 0.1 – 0.01 – 0.001 μg/mL). Transfected cells were stained by incubation for one hour at 4°C with the various antibodies. Cells were washed three times with staining buffer (1 x PBS, 0.2% BSA, 2 mM EDTA, 0.02% sodium azide) and then stained by incubation with a PE-conjugated goat anti-mouse secondary antibody (dilution 1/200) for 1 h at 4°C. Cells were washed three times, suspended in 150 μl of staining buffer and immediately analyzed by flow cytometry.

Surface plasmon resonance (SPR) experiments

SPR measurements were performed on a Biacore T100 apparatus (Biacore GE Healthcare) at 25°C. For FcγRs affinity studies, HBSEP+ (Biacore GE Healthcare) was used as the running buffer. NKCE-1 (NKp46/(Fc)/TA-NKCE-1), NKCE-2 (NKp46/Fc/TA-NKCE-2) and NKCE-3 (NKp46/Fc*/TA-NKCE-3) NKCEs were immobilized by covalent attachment to carboxyl groups on the surface of C1 Sensor Chips (GE Healthcare). The chip surface was activated by incubation with 1-ethyl-3-(3-dimethylaminopropyl) carbodiimide (EDC)/*N*-hydroxysuccinimide (NHS) (Biacore GE Healthcare). NKCEs were diluted to 10 μg/ml in coupling buffer (10 mM acetate, pH 5.2) and injected until the appropriate level of immobilization was achieved (i.e., 400 to 500 response units). The remaining activated groups were deactivated with 100 mM ethanolamine (pH 8) (Biacore GE Healthcare). Binding studies were performed with the classical kinetic wizard (as recommended by the manufacturer). Serial dilutions of soluble recombinant CD16aV (158V allele), CD16aF (158F allele), CD32a, CD32b, CD16b (from 61.7 to 5000 nM) and CD64 (from 0.74 to 60 nM) were injected over the NKCE–immobilized proteins and allowed to dissociate for 10 min before regeneration. In all experiments, EDC/NHS-activated and ethanolamine-deactivated flow cell 1 served as the reference for blank subtraction.

For the FcRn binding study, 150 mM NaCl in 20 mM sodium acetate pH 5.6 was used as the running buffer. FcRn recombinant proteins were immobilized covalently to carboxyl groups at the surface of C1 Sensor Chips. Serial dilutions of soluble control IgG1, F2, NKCE-1 and NKCE-2 NKCEs (from 20 to 320 nM) were injected over the FcRn–immobilized proteins and allowed to dissociate for 10 min before regeneration.

For NKp46 affinity studies, NKCE-1 (NKp46/(Fc)/TA-NKCE-1) and NKCE-2 (NKp46/Fc/TA-NKCE-2) NKCEs were diluted to 5 μg/ml in running buffer and injected onto protein-A chips until the appropriate level of capture was achieved (i.e., 80 to 100 response units). Binding studies were performed with the classical kinetic wizard (as recommended by the manufacturer). Serial dilutions of soluble NKp46 recombinant proteins (from 31 to 500 nM) were injected over the NKCE–captured proteins and allowed to dissociate for 10 min before regeneration.

For simultaneous NKp46 and CD16 binding, NKCE-3 (NKp46/Fc/TA-NKCE-3) NKCEs were diluted to 5 μg/ml in running buffer and injected onto protein-A chip until the appropriate level of capture was achieved (i.e., 400 to 500 response units). NKp46 recombinant proteins (at a concentration of 500 nM) were injected twice over the NKCE–captured proteins to ensure full saturation of NKCEs, and recombinant CD16a proteins (at a concentration of 1 μM) were injected over the NKCE-NKp46 complexes.

Production and purification of antibodies

The sequences encoding the light chain variable domains and heavy chain variable domains of the various antibodies were inserted into the SLX192 vector in frame with the desired human or mouse constant region. All the vectors were sent for sequencing before their use to transfect the CHO cell line and to generate pools and/or clones of antibody-producing cells. All the antibodies were purified from the supernatant with protein A beads. All the purified molecules were stored in 1 × PBS and analyzed to check for the absence of aggregates and endotoxins.

Titration of anti-NKp46 antibodies on human or cynomolgus NK cells

Human NK cells were purified from PBMCs by magnetic negative selection, with a human NK cell isolation kit (MACS-Miltenyi Biotec). About 100,000 NK cells were incubated with a dose-range of PE-conjugated anti-NKp46 antibodies for 1 h at 4°C, then washed three times with PBS, fixed with CellFix (BD) and acquired on a FACS CANTO II (BD).

Cynomolgus PBMCs were isolated from whole-blood samples by density gradient centrifugation in a Cell Preparation Tube (CPT™) with sodium citrate (BD Vacutainer). 170,000 cells were incubated with a dose range of anti-NKp46 antibodies for 1 h at 4°C and washed three times with PBS (Gibco). Cells were incubated for 30 minutes at 4°C with secondary goat-anti-human IgG (Fc)-PE Ab plus gating antibody mix containing anti-CD3-Pacific Blue (BD), anti-CD14-FITC (BD), anti-CD20-PerCP (Miltenyi Biotec),

anti-CD159a-APC (Beckman Coulter) antibodies, washed three times with PBS (Gibco) and fixed with CellFix (BD) for acquisition on a FACS CANTO II (BD).

Assay of NK cell cytotoxicity to tumor cell lines

NKCE-mediated tumor cell lysis by human NK cells (purified NK cells or KHYG-1 leukemia NK cells) was assessed in a standard chromium release assay. Briefly, PBMCs were isolated from buffy coats from healthy donors (EFS: *Etablissement Français du Sang*, Marseille) by centrifugation on Ficoll (GE Healthcare) density gradients. A preparation enriched in NK cells was obtained from PBMCs by magnetic negative selection, with a human NK cell isolation kit (MACS-Miltenyi Biotec), according to the manufacturer's instructions. NK cells described as "resting" were left overnight in culture medium before the assay. NK cells or KHYG-1 cells were plated with tumor cells (Daudi Burkitt's lymphoma, A549 lung adenocarcinoma or HUT78 cutaneous T-cell lymphoma) loaded with chromium-51 (^{51}Cr) (PerkinElmer) at an effector:target (E:T) cell ratio of 10:1 for NK cells and 20:1 for KHYG-1 cells in U-bottomed 96-well plates (BD Falcon). The same settings were used to assess NK cell mortality induced by NKCE. In this case, 50% of NK cells were loaded with ^{51}Cr and plated with cold tumor cells (Daudi) at an E:T cell ratio of 10:1. Dose ranges of NKCE molecules were added (in duplicate) and plates were incubated for 4 h at 37°C. After incubation, 50 µl of the culture supernatant was transferred to a LumaPlate (Perkin Elmer) coated with solid scintillator, which was then placed in a microplate scintillation counter (TopCount NXT, Perkin Elmer) to measure ^{51}Cr release into the supernatant, which was correlated with target cell lysis. The following formula was used to calculate the percent specific lysis:

$$specific\ lysis\ (\%) = \frac{(experimental\ release - spontaneous\ release)}{(maximal\ release - spontaneous\ release)} \times 100$$

The maximal release of ^{51}Cr was determined by adding 2% Triton X-100 (Sigma-Aldrich) to the target cells, and spontaneous release was measured in medium alone.

NKG2D and NKp46 expression levels were determined by flow cytometry, by incubating KHYG-1 or NK cells for 30 minutes with PE-conjugated anti-NKG2D (Beckman Coulter) or anti-NKp46 (Beckman Coulter) antibodies or isotypic controls. Cells were washed with PBS and fixed with CellFix for acquisition in a FACS CANTO II.

Activation of NK cells towards tumor cell lines

In one experiment, NK cell activation by NKCEs was assessed by flow cytometry with the CD107 degranulation marker and the CD69 activation marker. Human NK cells, purified as previously described, were co-incubated with or without Daudi cells at an E:T ratio of 2.5:1 for 4 h at 37°C, in the presence of various doses of antibodies or NKCEs. The cells were then washed twice in staining buffer (PBS (Gibco), 0.2% BSA (Sigma-Aldrich), 2 mM EDTA (Invitrogen) and 0.02% sodium azide (Sigma-Aldrich)) and stained with a mixture of anti-CD3-Pacific Blue (BD Pharmingen), anti-CD56-Pe-Vio770 (Miltenyi Biotec), anti-CD69-PE (Miltenyi Biotec), anti-CD107b-eFluor660 (eBioscience) and anti-CD107a-APC (BD Biosciences) antibodies for 30 min at 4°C. Cells were washed twice, fixed with CellFIX (BD) and data were acquired on a FACSCantoII (BD) flow cytometer. In another experiment, NK cell activation by NKCEs was determined by flow cytometry using CD107 degranulation marker, CD69 activation marker, TNF-α and IFN-γ secretion. Human resting NK cells, purified and cultured as previously described, were co-incubated with or without Daudi cells at an E:T ratio of 1:1 for 4h at 37°C, in the presence of a dose-range of antibodies or NKCE. GolgiStop (BD) was also added to the preparation to block intracellular protein transport process. After the incubation, cells were washed once in staining buffer and stained with a mix of anti-CD3-Pacific Blue (BD Pharmingen), -CD56-Pe-Vio770 (Miltenyi Biotec), -CD69-PE (Miltenyi Biotec), -CD107a-APC (Miltenyi Biotec) and -CD107b-APC (Miltenyi biotech) antibodies for 30 min at 4°C. Cells were washed twice, fixed and permeabilized with Cytofix/Cytoperm (BD). Cells were washed twice in Perm/Wash (BD) and stained with a mix of anti-TNF-BUV395 (BD Horizon) and -IFNγ-BV605 (Biolegend) antibodies for 30 min at 4°C. Cells were washed twice and data were acquired on a LSRFortessa X-20 (BD) flow cytometer.

Mouse tissue preparation and flow cytometry analysis

Peripheral blood was collected from the retro-orbital sinus of anesthetized mice into sodium heparin-coated hematocrit capillaries (Hirschmann-Laborgerate). For analysis of the NK cell population, immunofluorescence staining was performed with APC-anti-CD45 (30-F11, BD), VioBlue-anti-NKp46 (29A1.4, Miltenyi Biotec), and FITC-anti-CD3 (145-2C11, BD) antibodies, and erythrocytes were then lysed with Optilyse C lysis solution (Beckman Coulter).

Flow cytometry was performed with a FACS Canto or LSR FORTESSA X20 (BD) machine, equipped with BD FACSDiva software for acquisition. All data were analyzed with FlowJo software (Tree Star).

In vivo murine tumor experiments

For the solid tumor model, 5×10^6 Raji cells in a 1:1 mixture of endotoxin-free PBS and Matrigel (Corning) were injected s.c. into the flank of CB-17 SCID recipient mice. Tumor size was monitored with a digital caliper (Mitutoyo) every three to four days and is expressed as a volume ((length × width^2) /2). The tumor-bearing mice were randomized when tumor volume reached approximately 90–100 mm^3.

For the disseminated tumor model, 5×10^6 Raji cells were injected intravenously (i.v.) into the tail vein. The following day, the mice were randomized to different groups (n = 8–10) and the treatments were initiated. Mice were observed daily, to monitor clinical signs (hind limb paralysis, moribundity), and weighed two to three times per week. Mice that had lost at least 20% of their body weight were killed.

The antibody treatments were inoculated at various time points, i.v. (100 μL) or intraperitoneally (i.p.) (100 μL), at the doses indicated.

For NK cell depletion, 100 μL of polyclonal anti-asialo-GM1 (Poly21460, Biolegend) antibody was injected i.p. into recipient mice once weekly. Normal rabbit serum was administered as a control.

In situ hybridization

At each timepoint (d13; 2 days after treatment and d20; 2 days after treatment), primary tumors (n = 9 for each group treated with 1 x PBS, IC/(Fc)/CD20-NKCE-1 or NKp46/(Fc)/CD20-NKCE-1) were resected, fixed by incubation in 4% formalin for 24 h and embedded in paraffin. FFPE tissue blocks were sliced into 5 μm-thick sections and *in situ* hybridization was performed with RNAscope technology (Advanced Cell Diagnostics). All ISH staining was performed on a Bond Rx (Leica) according to the manufacturer's instructions. RNA quality was checked for each block with RNAscope 2.5 LS probes DapB (cat. #312038) and Mm-PPIB (cat. #313918), and tissue sections were then stained with RNAscope 2.5 LS probe Mm-Ncr1 (cat. #501728). Probes were detected with 2.5 LSx reagent kit - brown (cat. #322700). After staining, sections were dehydrated, cleared and coverslipped. Slides were scanned with a Nanozoomer S60 scanner (Hamamatsu).

Image analysis

IHC image analysis and quantification were performed with Halo software 1.0 (IndicaLabs). A random forest classification algorithm was used to distinguish between empty, necrotic and tissue areas within each individual spot of the TMA. The cytonuclear quantification module was used to assess $NKp46^+$ and $CD8^+$ cell densities in the classified tissue regions (number of NKp46 positive or CD8 positive cells/mm^2). ISH analysis was performed with Halo 2.0 software. Tumors were manually segmented by drawing a ROI to exclude the surrounding non-tumoral tissue from the analysis. A random forest classification algorithm was then used to distinguish between necrotic and tissue areas within the defined ROI. NCR1 probe detection was then quantified in classified tissue regions, with the ISH v. 2.2 module. Cells were considered positive if more than one probe was detected in the cytoplasm.

Protein production and purification for crystallization

Recombinant NKp46 was expressed as a secreted protein in Sf9 insect cells (Thermo Fisher Scientific), with the BAC TO BAC Baculovirus expression system (Thermo Fisher Scientific). Anti-NKp46-1 and anti-NKp46-4 antibodies were produced in CHO mammalian cells. Cells were harvested by centrifugation (4,000 x *g* for 10 min) and the supernatant was clarified by centrifugation (16,000 x *g* for 30 min) The proteins were purified from the culture supernatant by immobilized metal ion affinity chromatograph, with a 5 mL HisTrap ExcelGE Healthcare) Ni^{2+}- chelating column equilibrated in buffer A (20 mM Hepes pH 7.5, 150 mM NaCl, 5 mM imidazole). The proteins were eluted with buffer A supplemented with 250 mM imidazole and were further purified by size exclusion chromatography (HiLoad 16/60 Superdex 200 prep grade, GE) equilibrated in 20 mM Hepes pH 7.5, 150 mM NaCl. NKp46 and anti-NKp46-1 formed a complex with a 1:1 ratio, which was purified by size exclusion chromatography. Finally, Fab anti-NKp46-4 was added to NKp46-anti-NKp46-1 in a 1:1:1 ratio and purification by size exclusion chromatography was then performed. The purity of the protein was monitored at all stages of the purification process by SDS–PAGE (polyacrylamide gel electrophoresis) with visualization by Coomassie blue staining.

For crystallization trials, the purified proteins were concentrated by centrifugation in an Amicon 50 kDa cutoff concentrator, in the same buffer as for exclusion chromatography. The protein concentration was determined by measuring the absorbance of the sample at 280 nm with a NanoDrop 2000 spectrophotometer (Thermo Fisher Scientific).

Crystallization, data collection and processing

Initial crystallization trials for anti-NKP46-1 were performed by the sitting-drop vapor-diffusion method at 293 K in 96-well Swissci plates, with a Mosquito Crystal robot (TTP Labtech) and the following screens: the Pact Premier Screen (Molecular Dimensions), Stura screen (Molecular Dimensions) and Ammonium Sulfate Suite (Qiagen) .

Crystallization hit for anti-NKp46-1 (15.8 mg/mL) occurred in condition No. D6 of the Pact Premier screen [0.1 MMT pH 9, 25% PEG1500]. After optimization (Lartigue et al., 2003), the final crystallization conditions were 0.1 M MMT pH 8.5-9.5, 20-30%(w/v) PEG 1500. Diffraction data were collected to a resolution of 1.75Å on beamline Proxima-2A at SOLEIL, Paris, France. The data sets were integrated with XDS (Kabsch, 2010) and were scaled with SCALA (Evans, 2006) from CCP4 Suite (Winn et al., 2011). Data collection statistics are reported in Table S2.

Initial crystallization trials for the NKp46-1/anti-NKp46-1/anti-NKp46-4 complex were performed by the sitting-drop vapor-diffusion method at 293 K in 96-well Swissci plates, with a Mosquito Crystal robot (TTP Labtech) and the following screens: JCSG+ Suite (Qiagen), Morpheus (Molecular Dimensions), Ammonium Sulfate Suite (Qiagen) and Index (Hampton Research). Microcrystals were obtained in condition No. D1 of JCSG+suite and were used for microseeding in the Morpheus screen. Crystals of the complex (15 mg/mL) formed in condition N°. G9 of this Morpheus screen [0.1 M carboxylic acid, 0.1 M Tris/bicine pH 8.5, 50%

P500MME/P20k]. Diffraction data were collected at a resolution of 2.9Å on beamline Proxima-1 at SOLEIL, Paris, France. The data sets were integrated with XDS (Kabsch, 2010) and scaled with SCALA (Evans, 2006) from the CCP4 Suite (Winn et al., 2011). Data collection statistics are reported in Table S3.

Structure determination

The structure of the anti-NKp46-1 antibody was solved by molecular replacement with MOLREP (Vagin and Teplyakov, 2010) using the structure of Fab contained in the PDB entry 3T2N as a starting model. Refinement was performed with autoBUSTER (Blanc et al., 2004) and the structures were corrected with COOT (Emsley and Cowtan, 2004). The refinement statistics are reported in Table S2.

The structure of the complex between NKp46-1, anti-NKp46-1 and anti-NKp46-4 was solved by molecular replacement with MOLREP (Vagin and Teplyakov, 2010), using the structure of human NKp46 (PDB code 1OLL) and of the previously solved Fab anti-NKp46-1. Refinement was performed with autoBUSTER (Blanc et al., 2004) and the structures were corrected with COOT (Emsley and Cowtan, 2004). The refinement statistics are reported in Table S3.

Human NK cells, flow cytometry staining and t-SNE analysis

Head and neck tumor samples (Table S4) were cut into small pieces and incubated in 2 mL CO_2-independent medium containing 5% FBS, 200 μL collagenase I, 5 μL DNAse and 80 μL hyaluronidase, for 50 minutes at 37°C on a shaker (with homogenization by pipetting every 15 minutes). The cell suspension was filtered with a 40 μm cell strainer, and the cells were washed twice in PBS/2 mM EDTA/1% FBS at 4°C. The cells, as well as fresh whole blood from the head and neck cancer patients, were washed in PBS at 4°C before staining with Live/Dead aqua according to the manufacturer's instructions. They were then incubated with the cocktail of conjugated antibodies, and the red blood cells were lysed with BD FACS lysis buffer before acquisition on a BD LSR Fortessa flow cytometer. The compensated data were analyzed with FlowJo v10.5.2 either in a classical supervised manner (exclusion of aggregates/debris/ dead cells, gating of the NK, analysis of positivity and signal intensity for each marker), or in an unsupervised manner (export of NK events, equalization of cell numbers by DownSample plugin, concatenation, and analysis by t-SNE). For the t-SNE analysis, the clusters were defined manually after careful observation of cluster density changes between the blood and the tumor, independently of the expression of surface markers.

QUANTIFICATION AND STATISTICAL ANALYSIS

Detailed information concerning the statistical methods used is provided in the figure legends. Statistical analyses were performed with GraphPad Prism software version 7 (GraphPad) and R package lmerTest. R studio and the ggplot2 package were used to draw the violin plots with boxplots. Kaplan Meier methods were used for survival analysis. When sample size was sufficiently large, the normality of populations was assessed with the d'Agostino-Pearson omnibus normality test. If the data were not normally distributed, the statistical significance of differences between paired sample populations was determined with the Wilcoxon matched-pair signed rank test for three or more groups. *N* is the number of samples used in the experiments. The means or medians are shown, with or without error bars indicating the SD.

We used *t* tests to compare two groups with normally distributed continuous variables, and Mann-Whitney tests to compare two groups with non-normally distributed continuous variables. We used one-way ANOVA followed by Tukey's multiple comparisons tests to analyze experiments with more than two groups with normally distributed continuous variables. For non-normally distributed data, we performed one-way ANOVA followed by Dunn's multiple comparisons test. A linear mixed-effects model was applied to estimate tumor growth and differences between treatments. Treatment and days were defined as fixed effects and mouse as random effects. Pairwise differences of LS-mean were computed for the Treatment factor. P-values were calculated based on the t-distribution using degrees of freedom based on Kenward-Roger method. These calculations were done with the R package lmerTest. Significance is indicated as follows: $*p < 0.05$; $**p \leq 0.01$; $***p < 0.001$, $****p < 0.0001$.

Four-parameter non-linear regression analysis was used to calculate the anti-NKp46 or NKCE EC_{50}.

DATA AND SOFTWARE AVAILABILITY

X-ray crystallography data

The accession number for the structure of Anti-NKp46 antibody NKp46-1 reported in this paper is Protein Data Bank (PDB): 6IAS. The accession number for the structure of human NKp46 in complex with antibody NKp46-1 and NKp46-4 reported in this paper is PDB: 6IAP.

Protein Data Bank: https://www.rcsb.org/

Softwares and algorithms

FlowJo version 10.5: https://www.flowjo.com/solutions/flowjo/

Flow cytometry data analysis.

GraphPad Prism version 7.00: https://www.graphpad.com/scientific-software/prism/

Data analysis and presentation.

BD FACSDiva Software 8.0: https://www.bdbiosciences.com/in/instruments/software/facsdiva/
Data acquisition and analysis by flow cytometry.
Halo 1.0 and 2.0: http://www.indicalab.com/
Image analysis.
R studio version 3.5.1: https://www.rstudio.com/
Statistical computing.
Fiji: https://fiji.sc/
Image processing package.
XDS: http://xds.mpimf-heidelberg.mpg.de/html_doc/downloading.html
Program for processing rotation images using a single cpu at each cluster node
SCALA: http://www.ccp4.ac.uk/html/scala.html
Program for scaling together multiple observations of reflections and merging multiple observations into an average intensity.
CCP4: http://www.ccp4.ac.uk/
Integrated suite of programs to determine macromolecular structures by X-ray crystallography
MolREP: http://www.ccp4.ac.uk/html/molrep.html
Automated program for molecular replacement.
AutoBuster: https://www.globalphasing.com/buster/
Structure refinement.
COOT: https://www2.mrc-lmb.cam.ac.uk/personal/pemsley/coot/
Macromolecular model building, model completion and validation.
Molprobity: http://molprobity.manchester.ac.uk/
Structure validation.

Cell

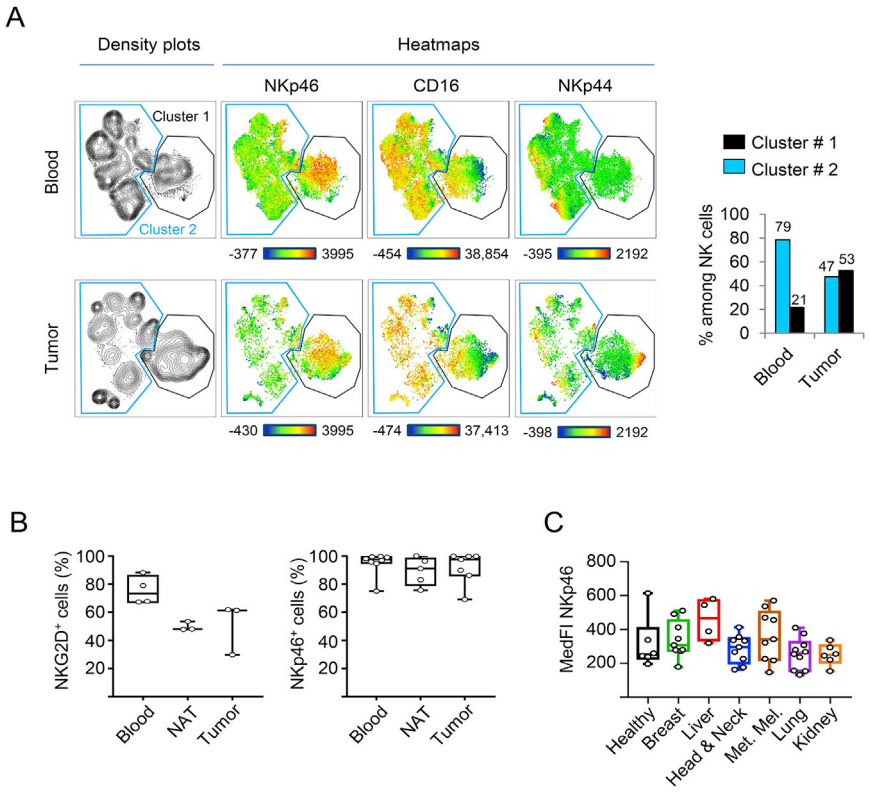

Figure S1. NKp46 Expression Is Not Downregulated in Cancer, Related to Figure 1.

(A) t-SNE analysis of NK cells from peripheral blood (pooled patients n = 23), and tumor tissue (pooled patients n = 13) from head and neck cancer patients. Data show cell distribution as density plot (left panel) and histogram (right panel). Tumor-enriched cluster #1 is delineated (in black) relative to cluster #2 (in blue). Histograms show the cluster composition of NK cell populations in tissues. Color-coded heatmaps show the relative staining intensity for each marker (lowest intensity in blue, highest in red).

(B) Flow cytometry study showing the percentage of NKG2D- and NKp46-positive NK cells in blood (Blood; n = 4 and 8), normal tissues adjacent to the tumor (NAT; n = 3 and 5) and tumors (Tumor; n = 3 and 7) from lung cancer patients.

(C) Median fluorescence intensity for NKp46 staining, on the flow cytometry of peripheral NK cells from cancer patients and healthy donors. Healthy donors (healthy; n = 6). Breast (n = 9). Liver (n = 4). Head and Neck (n = 9). Metastatic melanoma (Met. Mel; n = 9). Lung (n = 10). Kidney (n = 6).

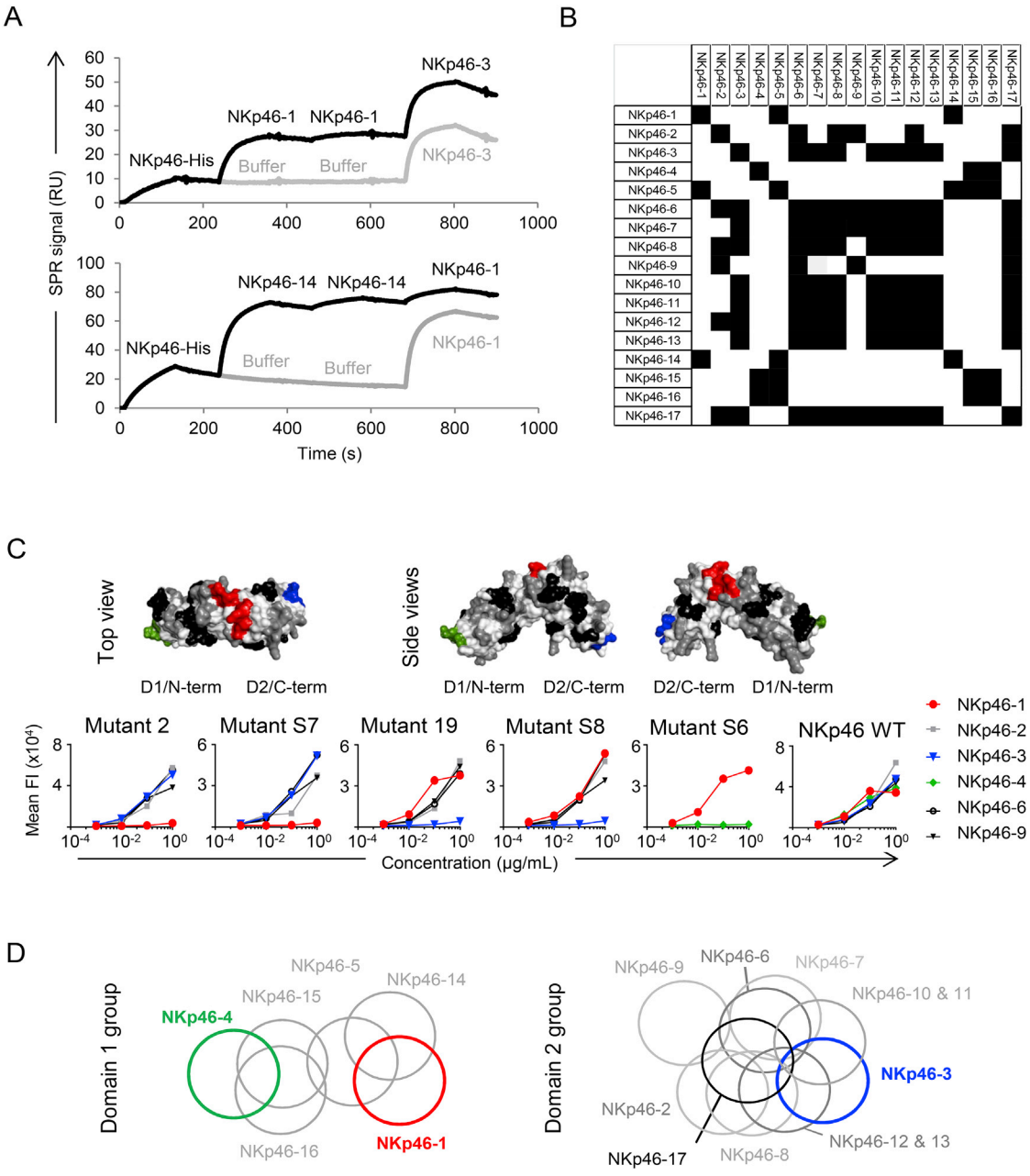

Figure S2. Anti-NKp46 mAb Epitope Characterization, Related to Figure 1

(A) Sensorgrams showing the binding of a second anti-NKp46 antibody to captured NKp46 proteins saturated by two injections of a first antibody (black) or in the absence of the first antibody (gray) were superimposed and aligned with zero on the *x* and *y* axis at the start of capture injection. (upper panel) Representative sensorgrams for non-competing antibodies. (lower panel) Representative sensorgrams for competing antibodies.

(B) Competition matrix built from SPR data. Black squares: competing antibodies; white squares: non-competing antibodies. All pairs of antibodies displayed symmetric behavior except NKp46-7 and -9.

(C) Epitope mapping study: (upper panel) mutated residues at the molecular surface of human NKp46. Gray: mutants 1 to 23; black: mutants S1 to S13; red: mutants 2 and S7; blue: mutants 19 and S8. (Lower panel) data from representative flow cytometry experiments assessing anti-NKp46 mAb binding to HEK cells engineered to express wild-type NKp46 or mutants 2, 19, S6, S7, and S8.

(D) Epitope diagram built from the results of the SPR competition study. Epitopes are represented as circles. Overlapping circles indicate that antibodies compete.

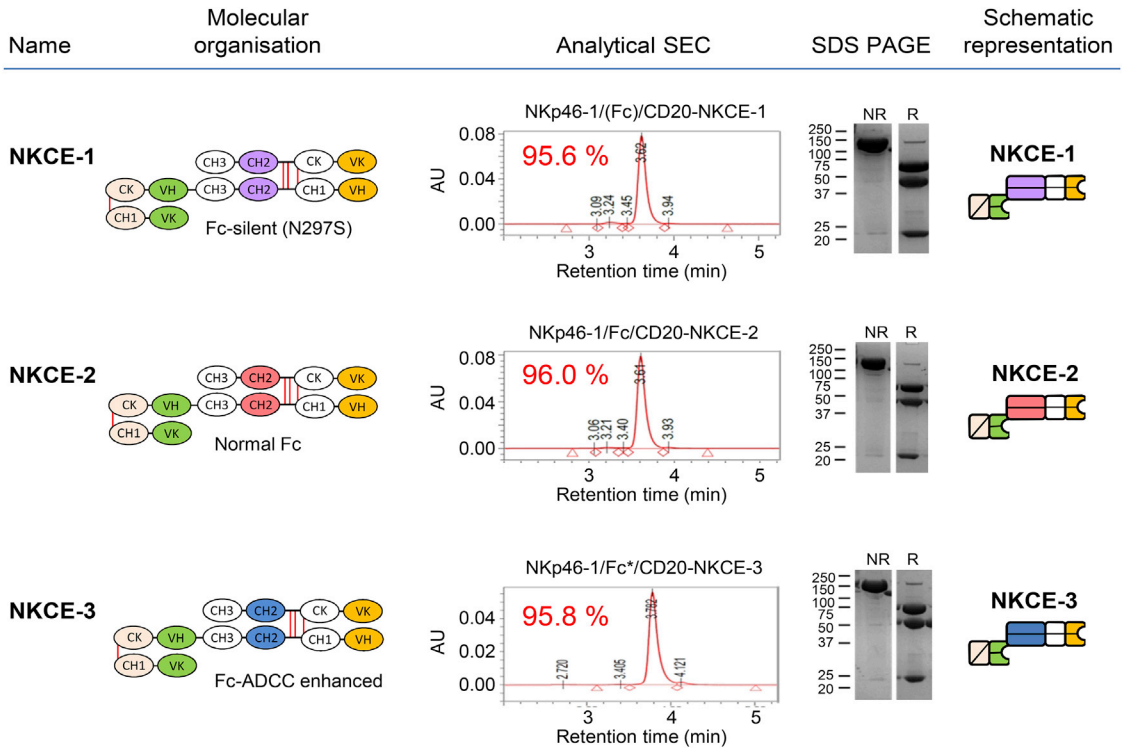

Figure S3. Production and Purification of NKCEs, Related to Figure 3

Data show SEC and SDS-PAGE profiles for the different NKCEs. First column: format name. Second column: molecular design of the NKCEs. Third column: analytical size exclusion chromatography (SEC) on the final product after Protein-A and SEC purification. Purity is indicated on each chromatogram, with optical density at 280 nm (AU) represented as a function of retention time in minutes. Fourth column: electrophoretic profiles under non-reducing (NR) or reducing (R) conditions on SDS-PAGE with Coomassie brilliant blue staining. Fifth column: schematic diagram of the NKCEs.

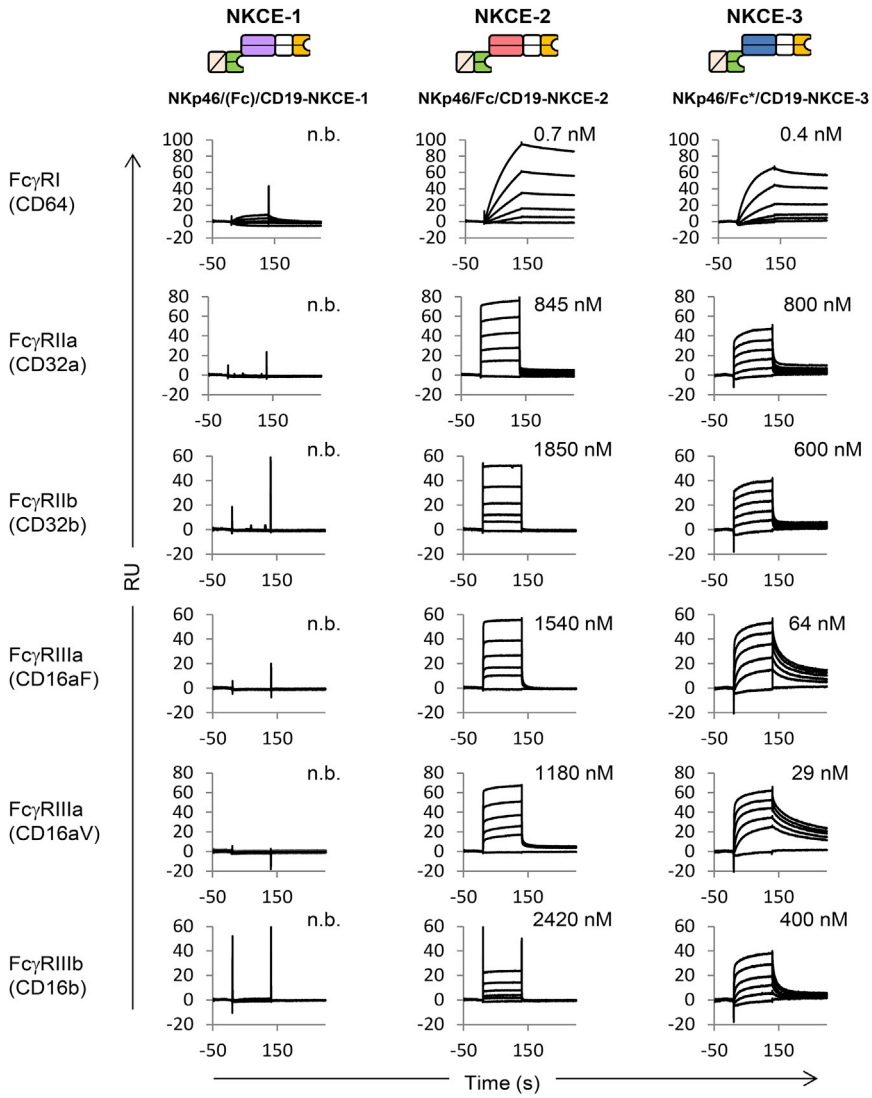

Figure S4. Affinity of the Various Fc Fragments for Fc-Gamma Receptors, Related to Figure 3

Study of the binding affinity of NKCE-1 (NKp46/(Fc)/TA–NKCE-1) (left panels), NKCE-2 (NKp46/Fc/TA-NKCE-2) (middle panels) and NKCE-3 (NKp46/Fc*/TA-NKCE-3) (right panels) NKCEs for human Fc-gamma receptors, as determined by SPR. Superimposed sensorgrams of CD16aF (158F allele), CD16aV (158V allele), CD16b, CD32a, and CD32b serial dilution (from 5000 to 61.7 nM) and of CD64 serial dilution (from 60 to 0.74 nM) were aligned with 0 on the x and y axes at the start of injection. K_D values are shown. The data shown are representative of 3 independent experiments.

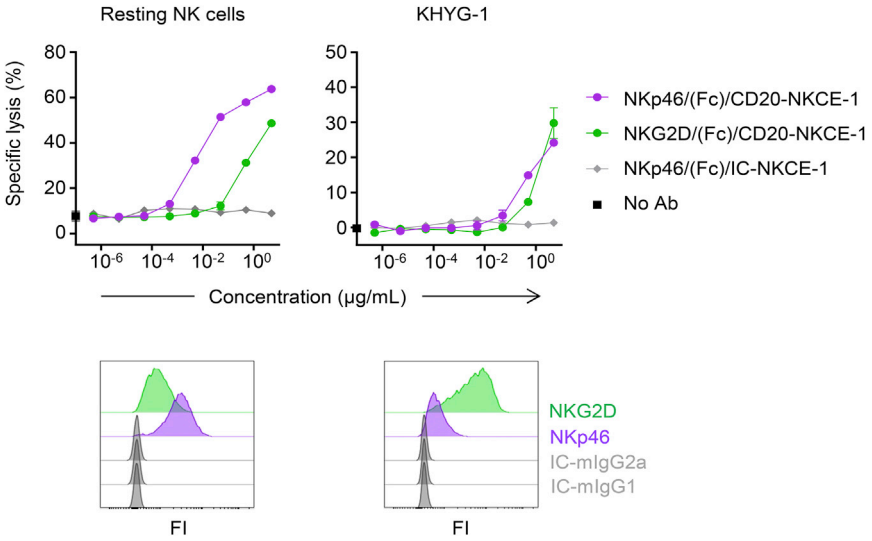

Figure S5. NKCEs Targeting NKp46 Promote NK-Cell-Mediated Tumor Lysis More Efficiently than Those Targeting NKG2D, Related to Figure 3

Comparative cytotoxicities of NKp46- and NKG2D-NKCEs against Daudi targets with purified resting NK cells (left panels) and the KHYG-1 NK cell line (right panels). Flow cytometry profiles show expression levels of NKp46 and NKG2D on resting NK cells (left) and KHYG-1 cells (right).

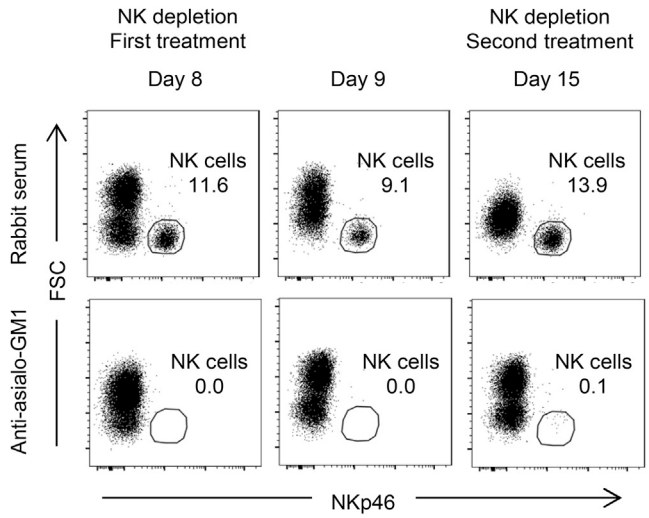

Figure S6. Depletion of Mouse NK Cells by Anti-Asialo-GM1 Antibody Treatment, Related to Figure 4

NK cell depletion was followed, on days 8 (first treatment), 9 and 15 (second treatment) by flow cytometry analysis of the PBMCs of mice treated with control rabbit serum (upper panels) or anti-asialo-GM1 antibody (lower panels). The percentage of circulating NK cells is indicated.

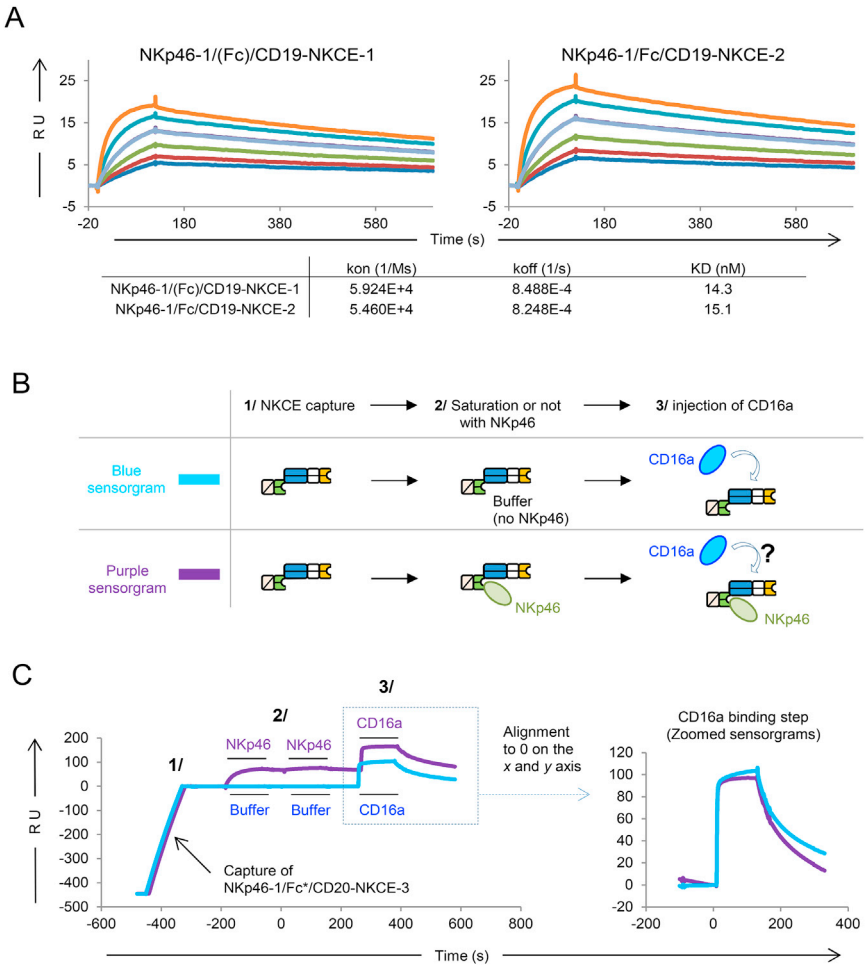

	kon (1/Ms)	koff (1/s)	KD (nM)
NKp46-1/(Fc)/CD19-NKCE-1	5.924E+4	8.488E-4	14.3
NKp46-1/Fc/CD19-NKCE-2	5.460E+4	8.248E-4	15.1

Figure S7. Fc-Competent and Fc-Silent NKCEs Bind to NKp46 with Similar Affinity and Fc-Competent NKCEs Can Simultaneously Co-engage CD16 and NKp46, Related to Figure 5

(A) Affinity study. Superimposed sensorgrams showing the binding of NKp46 recombinant proteins to NKp46-1/(Fc)/CD19-NKCE-1 (left) and NKp46-1/Fc/CD19-NKCE-2 (right) captured on a Protein-A chip. We fitted a 1:1 binding model to the data.

(B and C) Binding of NKp46 and CD16 to NKCE-NKCE-3. (B) Experimental setting used in (C): (1) Capture of NKCEs on Protein-A. (2) Saturation of NKCEs by two injections of NKp46 proteins (purple) or running buffer (blue). (3) Injection of CD16a proteins onto NKp46-NKCE complexes (purple) or nude NKCEs (blue). (C) Left: Superimposed sensorgrams showing the successive injection steps. Right: Superimposed sensorgrams showing the binding of CD16a proteins to NKp46-NKCE complexes or nude NKCEs after the sensorgrams were aligned such that the CD16a injection start was at zero on the x and y axes.